JGR Biogeosciences

RESEARCH ARTICLE
10.1029/2019JG005387

Development, Productivity, and Seasonality of Living Planktonic Foraminiferal Faunas and *Limacina helicina* in an Area of Intense Methane Seepage in the Barents Sea

Siri Ofstad[1], Julie Meilland[2], Katarzyna Zamelczyk[1,3], Melissa Chierici[4], Agneta Fransson[3], Friederike Gründger[5], and Tine L. Rasmussen[1]

[1]CAGE—Centre for Arctic Gas Hydrate, Environment and Climate, Department of Geosciences, UiT, The Arctic University of Norway, Tromsø, Norway, [2]MARUM—Center for Marine Environmental Sciences, University of Bremen, Bremen, Germany, [3]Norwegian Polar Institute, Fram Centre, Tromsø, Norway, [4]Institute of Marine Research, Tromsø, Norway, [5]Arctic Research Centre, Department of Bioscience, Aarhus University, Aarhus, Denmark

Key Points:
- Planktonic foraminifera and *Limacina helicina* increase in size and concentration (no. individuals m^{-3}) from spring to summer
- Methane plumes coincided with elevated dissolved inorganic carbon, low pH, and calcium carbonate saturation Ω
- No link was found between methane and planktonic foraminifera and *Limacina helicina* concentrations

Supporting Information:
- Supporting Information S1

Correspondence to:
S. Ofstad,
siri.ofstad@uit.no

Citation:
Ofstad, S., Meilland, J., Zamelczyk, K., Chierici, M., Fransson, A., Gründger, F., & Rasmussen, T. L. (2020). Development, productivity, and seasonality of living planktonic foraminiferal faunas and *Limacina helicina* in an area of intense methane seepage in the Barents Sea. *Journal of Geophysical Research: Biogeosciences*, *125*, e2019JG005387. https://doi.org/10.1029/2019JG005387

Received 19 JUL 2019
Accepted 6 FEB 2020
Accepted article online 9 FEB 2020

Abstract Although the plankton communities in the Barents Sea have been intensely studied for decades, little is known about the living planktonic foraminiferal (LPF) and pteropod faunas, especially those found at methane seep sites. Along a repeated transect in the "crater area" (northern Barents Sea, 74.9°N, 27.7°E) in spring and summer 2016 the flux of LPF and of the pteropod species *Limacina helicina* showed a high degree of variability. The LPF had low concentration (0–6 individuals m^{-3}) and small tests ($\bar{x}$ = 103.3 μm) in spring and a 53-fold increase (43–436 individuals m^{-3}) and larger tests ($\bar{x}$ = 188.6 μm) in summer. Similarly, the concentration of *L. helicina* showed a tenfold increase between spring and summer. The LPF species composition remained stable with the exception of the appearance of subtropical species in summer. No relationship was observed between the spatial distribution of LPF, *L. helicina*, and methane concentrations in the area. The methane plumes in April coincided with elevated dissolved inorganic carbon, low pH, and calcium carbonate saturation states, and the methane concentration seemed to be controlled by lateral advection. The $\delta^{13}C$ and $\delta^{18}O$ of *Neogloboquadrina pachyderma* and *Turborotalita quinqueloba* are comparable to previous observations in the Arctic and do not show any influence of methane in the isotopic signals of the shells. Although no evidence of direct impact of high methane concentrations on the LPF (size and concentration) were found, we speculate that methane could indirectly enhance primary productivity, and thus biomass, through several potential pathways.

Plain Language Summary Planktonic foraminifera and the thecosome pteropod species *Limacina helicina* are microscopic organisms who live in the water column and build their shells out of calcium carbonate. Little is known about the planktonic foraminiferal faunas in the Barents Sea, and their seasonality in general. This study is the first on planktonic foraminifera and *Limacina helicina* in an area of intense methane seepage from the seafloor. Sampling at sea took place during spring and summer 2016. We found a significant increase in shell size and concentration (individuals m^{-3}) in both planktonic foraminifera and *Limacina helicina* between spring and summer. In spring, carbon dioxide was being added from the methane plumes, altering the sea-water chemistry at the site of methane release. The addition of carbon dioxide could stimulate primary production in the overlying water column. However, we did not find that the spatial distribution of planktonic foraminifera coincided with where the methane concentration was the highest, or that methane concentration coincided with the elevation of primary production indicators. This study sheds light on the planktonic foraminifera community and their seasonal development in the Barents Sea for the first time with stratified net samples.

1. Introduction

Humankind's industrial and agricultural activities since the mid-18th century have caused an increase in atmospheric carbon dioxide (CO_2) from ~280 parts per million (ppm) to the present level, which exceeds 400 ppm (Dlugokencky & Tans, 2019; IPCC: Climate change, 2013). The consensus is that this anthropogenic increase in atmospheric CO_2 has had significant effects on Earth's climate, in particular at high latitudes (IPCC: Climate change, 2013). The polar oceans are very sensitive to the increased temperature and

atmospheric CO_2 (Orr et al., 2005; Stouffer et al., 1989). Consequently, the Arctic Ocean has transformed over the past decades, experiencing, among other processes, loss of sea ice (e.g., Stroeve et al., 2012), freshening (Haine et al., 2015; Rabe et al., 2011), ocean acidification (e.g., AMAP: AMAP assessment, 2013, AMAP: AMAP Assessment, 2018), an increase in primary production (Arrigo & van Dijken, 2011, 2015), and introduction of tropical and subtropical species at high latitudes (e.g., Bjørklund et al., 2012; Fossheim et al., 2015). All of these processes may have far-reaching effects on the entirety of the Arctic food chain, and hence will have socioeconomic repercussions (AMAP: AMAP Assessment, 2018).

If the current trend in global emissions of CO_2 continues, the pH of the oceans is predicted to decrease 0.3–0.5 units by the end of the century (Caldeira & Wickett, 2005). The Arctic Ocean will see the most dramatic effects, due to it being an especially strong CO_2 sink as a result of cold surface water, high biological productivity, seasonal freshwater inputs, and decreasing sea-ice cover (Bates & Mathis, 2009; Fransson et al., 2009; Kaltin & Anderson, 2005). Furthermore, shell dissolution and a range of other negative physiological responses may occur in calcifying planktonic organisms at high partial pressure of CO_2 (pCO_2), especially in combination with increased temperature. Pteropods (Bednarsek et al., 2014; Bednaršek et al., 2012; Comeau et al., 2009; Lischka et al., 2011) and planktonic foraminifera are considered to be especially vulnerable to ocean acidification (e.g., Davis et al., 2017; Manno et al., 2012; Moy et al., 2009). The reproduction rates of living planktonic foraminifera (LPF) change in response to changes in the environment with higher rates under favorable conditions and vice versa (Kucera, 2007). The global LPF community has changed since preindustrial times in terms of the spatial distribution of assemblages (Jonkers et al., 2019). The shift in the global LPF community is consistent with recent changes in temperature, demonstrating the sensitivity of the LPF to environmental conditions (Jonkers et al., 2019). Yet our understanding of LPF ecology is fragmented, especially in the northern polar regions. Little is known about causes of interannual variability in production in terms of absolute abundance (concentration) and species distribution patterns (e.g., Schiebel, 2002; Schiebel & Hemleben, 2000), the controls of vertical habitat changes (Greco et al., 2019; Kretschmer et al., 2018; Rebotim et al., 2017), and how the vertical habitat varies ontogenetically (Bijma et al., 1990; Hemleben et al., 1989; Schiebel et al., 1997). Also, linkage between the reproduction cycle of the LPF and the lunar cycle is barely known (Bijma et al., 1990; Erez et al., 1991; Hemleben et al., 1989; Jonkers et al., 2015; Schiebel & Hemleben, 2017; Volkmann, 2000). To complicate matters further, the extent to which different ecological parameters affect the production and distribution of LPF vary at species level (Schiebel & Hemleben, 2017). Lastly, it is not known whether or not the dominant Arctic species, *Neogloboquadrina pachyderma*, can overwinter in brine channels in pack and fast ice, as they do in the Southern Ocean (Dieckmann et al., 1991; Spindler, 1996). All of this leads to uncertainties when it comes to using planktonic foraminifers as a proxy for paleoclimate.

In the Arctic, gas hydrate provinces are widespread on the continental shelves (Damm et al., 2005; Graves et al., 2015; Mau et al., 2017; Pisso et al., 2016; Sapart et al., 2017; Shakhova et al., 2010; Westbrook et al., 2009) and are stable under low temperature and high pressure, this stability is threatened under the current climate warming trend. At present, little of the methane (CH_4) from the gas hydrate provinces reach the atmosphere (Graves et al., 2015; Pisso et al., 2016; Silyakova et al., 2015). Instead, the CH_4 from Arctic subsurface marine hydrate reserves is either anaerobically or aerobically oxidized in the upper layers of the sediments or in the water column by microbial activity (Boetius & Wenzhöfer, 2013; Ruppel & Kessler, 2017). In the water column, microbial aerobic oxidation (MO_X) and the less common AOM (anaerobic oxidation of methane) are sinks for CH_4; both processes remain poorly understood (Reeburgh, 2013). Following the release of CH_4 from the seafloor, these water column processes can change the manner of impact of the CH_4 release. For example, model studies have shown that, through the MO_X reaction, CH_4 seepage is a potential source of CO_2, which can increase ocean acidification (Biastoch et al., 2011; Archer et al., 2008). It has also been hypothesized that CH_4 seepage can cause an increase in photosynthetic primary production (Pohlman et al., 2017), making CH_4 seepage areas CO_2 sinks. There have been several studies in the Arctic focusing on the effects of CH_4 seepage on the living benthic communities (Åström et al., 2016, 2018, 2019; Sen, Duperron, et al., 2018, Sen et al., 2019), including living benthic foraminifera, although not exclusive to the Arctic region (Heinz et al., 2005; Herguera et al., 2014; Hill et al., 2004; Rathburn et al., 2000). However, no studies from the Arctic exist that examine the effects of CH_4 seepage on the pelagic ecosystem.

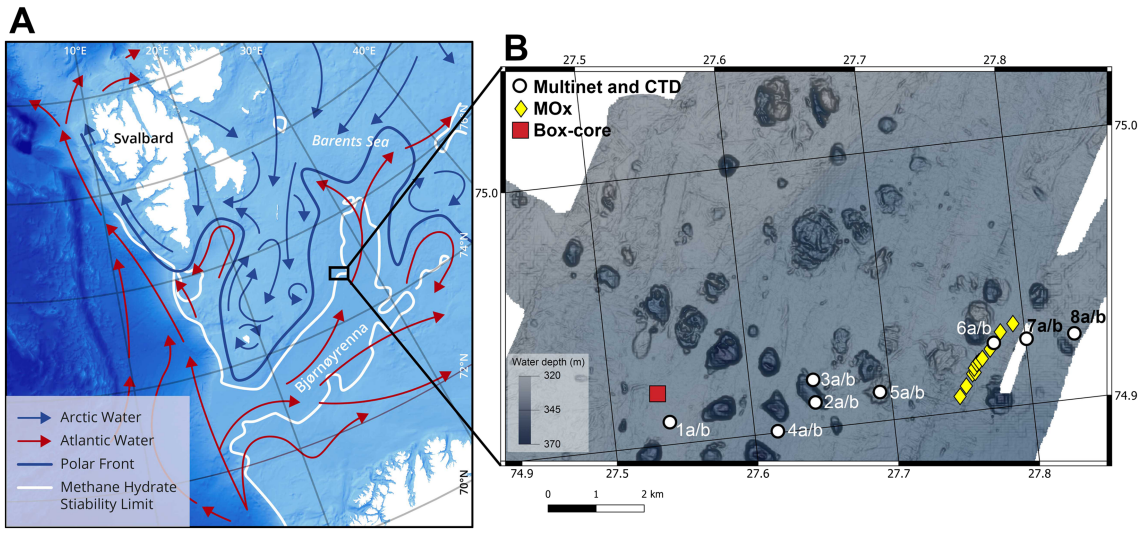

Figure 1. (a) Map of study area located in the northern Barents Sea, on the edge of the methane hydrate stability zone. Currents and polar front after Loeng (1991), methane hydrate stability limit after Andreassen et al. (2017). Study area is enclosed in black rectangle. (b) Multibeam bathymetry of the transect area (modified from Andreassen et al., 2017). White dots mark multinet and CTD sampling stations, yellow diamonds MO_X measurement stations, and red square the box-core location.

Here we aim to improve our understanding of the response of LPF and pteropods to seasonal changes and CH_4 release to the water column in the Barents Sea with focus on the species compositions, size, and concentration of specimens. This is the first study of LPF in an environment exposed to CH_4 seepage from the seafloor. We study the communities between spring (April) and summer (June) to further our knowledge of seasonal variability and eventual impact of CH_4 release an extremely variable chemical environment. Changes in size and concentrations of the LPF population are compared to equivalent data from the dominant species of pteropods *Limacina helicina*. We conducted two sampling campaigns in Arctic spring and summer, collecting samples from the Bjørnøyrenna crater area, which is located in the northern Barents Sea. This area is characterized by more than a hundred giant crater-mound systems, with high levels of CH_4 release from gas hydrates to the water column, with flares of up to 200 m height (Andreassen et al., 2017).

2. Study Area and Sampling Locations

The Barents Sea is a relatively shallow continental shelf sea dominated by the warm north-easterly flowing Atlantic Current, a branch of the Norwegian Atlantic Current called the North Cape Current (Loeng, 1991). The Bjørnøyrenna crater area (referred to in this study as the "crater area") (74.91°N, 27.7°E; Figure 1) is located in shallow water (~340 m depth) on the northern flank of Bear Island Trough, which is on the upper boundary of the gas hydrate stability zone (Andreassen et al., 2017) (Figure 1a). The crater area is ice-free year-round. During our sampling campaigns, the predominant water masses were Atlantic Water (AW, T > 3.0 °C, S > 34.65) (<300 m in April and <250 m in June) and Transformed Atlantic Water (TAW, T = 1.0–3.0 °C, S > 34.65) (>300 m in April and >250 m in June), following the definitions of Cottier et al. (2005). The study site has an area of about 440 km^2. Streams of gas bubbles entering the water column were visually observed by the ROV 30K during the CAGE 16-5 cruise in June 2016, and by hydroacoustics (EK60) during the CAGE 16-2 cruise in April 2016. Measurements have revealed that the CH_4 is primarily of thermogenic origin (Andreassen et al., 2017).

Seasonal sampling took place during two expeditions with *R/V Helmer Hanssen* in spring (CAGE 16-2, 15 April to 22 April) and summer (CAGE 16-5, 16 June 2016 to 4 July) 2016. On 19 April (spring), eight CTD (conductivity, temperature, depth) stations and a stratified plankton net were conducted across a 9 km transect (74.91°N, 27.5–27.9°E) located above several craters and mounds actively releasing CH_4 (Figure 1b). The sampling procedures were repeated on 29–30 June (summer), 71 days after the first sampling, with the

addition of aerobic methane oxidation (MO_X) rate and CH_4 measurements at 11 stations (74.91–74.92°N, 27.74–27.8°E) (Figure 1b). Also in June, three additional water samples were taken from a blade core at station 1b guided by a ROV just above the sediment-water interface for determining the CO_2 system (i.e., Total alkalinity (A_T) and Dissolved Inorganic carbon (DIC)). A surface sediment sample (position 74.92°N, 27.53° E) was retrieved using a box corer (Figure 1b).

3. Material and Methods

3.1. Environmental Parameters

Salinity, temperature, and depth in the water column were measured using a CTD (Sea-Bird SBE 19+) equipped with sensors for dissolved oxygen (DO) (Sea-Bird SBE 43) and chlorophyll *a*-fluorescence (chlfluo) (Sea-Bird ECO) (both indicators for primary production), and 12 × 5 L Teflon-lined Niskin bottles for water sampling. Water samples were collected at nine depths (5, 10, 25, 50, 100, 150, 200, 250 m, bottom), and were used for determining A_T, DIC, and CH_4. The water was transferred into Pyrex borosilicate bottles (250 ml) for the CO_2 system, and into crimp-top glass bottles (120 ml) for CH_4 concentration. Both parameters were sampled via a Tygon tube to prevent contact with air and to avoid gas bubbles. Samples for CH_4 analysis were collected immediately upon recovery of the CTD rosette. Also immediately after sampling, water samples for the CO_2 system were preserved with 60 µl of saturated mercury chloride ($HgCl_2$), CH_4 samples were amended with 1 ml of 1 M NaOH solution and capped with butyl rubber stoppers and crimped. Water samples were stored in the dark at 2 °C until analysis. The water from the blade core was sampled immediately after retrieval using a Tygon tube and preserved in the same way as the water samples taken by the CTD.

The water samples for the CO_2 system were analyzed for A_T and DIC at the Institute of Marine Research (IMR Tromsø, Norway). The method used is described in detail in Dickson et al. (2007). In short, DIC was determined using gas extraction of acidified samples followed by colorimetric titration and photometric detection using a Versatile Instrument for the Determination of Titration Alkalinity (VINDTA 3D, Marianda, Germany). The A_T was determined by potentiometric titration with 0.1 N hydrochloric acid using a Versatile Instrument for the Determination of Titration Alkalinity (VINDTA 3S, Marianda, Germany). Routine analyses of Certified Reference Materials (CRM, provided by A. G. Dickson, Scripps Institution of Oceanography, United States) were used to perform accuracy control. The accuracy of the measurements was better than ±1 and ±2 µmol kg^{-1} for DIC and A_T, respectively.

The remaining parameters of the CO_2 system of pH, fugacity of CO_2 (fCO_2), and aragonite saturation (Ω_{Ar}) were calculated using a CO_2-chemical speciation model (CO2SYS program, version 01.05) (Lewis & Wallace, 1998; Pierrot & Wallace, 2006) and the DIC and A_T measurements, in combination with temperature, salinity, and depth (pressure). The equilibrium constants K1, K2 from Mehrbach et al. (1973) refitted by Dickson and Millero (1987), and the total hydrogen-ion scale (pHT) were used. We used the HSO_4^- dissociation constant of Dickson (1990), and the boric acid dissociation constant of Uppström (1974).

Methane concentrations were determined using the headspace technique, described in detail in Berndt et al. (2014) and Steinle et al. (2015). In short, 5 ml of pure N_2 was added into each of the 120 ml glass bottles and shaken vigorously. Samples were stored in the fridge (2 °C) for 0.5 to 2 hr, allowing the dissolved gas in the seawater to equilibrate with the headspace gas. Following this, 2 ml of gas was extracted and analyzed by a ThermoScientific Trace 1300 gas chromatograph equipped with a flame ionization detector (GC-FID). Methane concentrations were determined according to Wiesenburg and Guinasso (1979).

3.2. Aerobic Methane Oxidation Rates

Aerobic methane oxidation (MO_X) is mediated by bacteria and proceeds according to the following net reaction:

$$CH_4 + 2O_2 \rightleftharpoons CO_2 + 2H_2O \quad (1)$$

Water samples were taken at 11 stations along a transect (Figure 1b) from eight different water levels, which were at 5, 15, 25 m below the sea surface, 5, 15, 25 m above seafloor, and two additional intermediate levels depending on water depth. Subsamples were taken immediately upon recovery of the sampler. MO_X rates were determined by ex-situ incubations with trace amounts of tritium labeled CH_4 (C^3H_4), allowing to

trace the label transfer by measuring the activity of substrate (C^3H_4) and product pools (^3H_2O) after incubation (Berndt et al., 2014; Niemann et al., 2015; Steinle et al., 2015). Briefly, for each sampling depth, six 20-ml crimp-top vials were filled and closed bubble-free with PTFE-coated Bromobutyl rubber stoppers (Wheaton, United States). Each sample was amended with 5 μl gaseous tritium-labeled CH_4 (C^3H_4) (~20 kBq, American Radiolabeled Chemicals, United States) and incubated for 72 hr at 4 °C in the dark. The incubations were terminated by adding 0.5 ml saturated $HgCl_2$ solution to one triplicate of the six parallel samples (aboard ship) and total activity ($^3H–CH_4 + {}^3H–H_2O$) was determined on a 2-ml aliquot mixed with 3 ml of scintillation cocktail (Ultima Gold, Perkin Elmer) by using a Liquid Scintillation Analyzer Packard TRI-CARB 2300TR (PerkinElmer, IL, United States) at our home laboratory. The remaining triplicate of samples was used to estimate the net amount of $^3H–CH_4$ consumption. Therefore, a 10-ml aliquot of the incubation was amended with aqueous NaCl solution (1 ml, 30%, w/v) and purged for 30 min with air to strip out the remaining CH_4. The activity of the produced ^3H_2O was determined in our home laboratories by liquid scintillation counting. MO_X rates were calculated from the fractional turnover of labeled CH_4 and measured water column CH_4 concentration assuming first order kinetics (Reeburgh, 2013):

$$rMO_X = k \times [CH_4], \tag{2}$$

where k is the first-order rate constant (determined from the fractional turnover of labeled CH_4 per unit time and corrected for tracer turnover in control samples) and $[CH_4]$ is the concentration of CH_4 at the beginning of the incubation. MO_X rates were corrected for insubstantial tracer turnover in control samples, which were taken frequently, fixed with $HgCl_2$ solution immediately after the addition of the tracer.

3.3. Plankton Samples Collection and Treatment

Foraminiferal and thecosome pteropod specimens were sampled concurrent with the hydrographic samples using a Multinet with mesh size of 64 μm (net opening 0.5 m^2; Hydro-Bios, Kiel, Germany). This mesh size enabled the collection of small specimens, possibly preadults, in order to address seasonality and reproduction between the two sampling campaigns. The nets were towed vertically, collecting plankton at five consecutive depth intervals (300–200, 200–150, 150–100, 100–50, and 50–0 m) (Table S1). The flowmeter attached to the net opening allowed calculation of the volume of water filtered through each net and calculation of concentration of specimens (number individuals/volume (m^{-3})). Once on board, the samples were sieved with sea water through a 63-μm sieve and transferred into plastic bottles (250 ml) where they were immediately fixed and buffered with approximately 230 ml ethanol (98%), a quarter of a teaspoon hexamethylenetetramine (≥99.0%), and stored at 2 °C. Once returned to the home laboratory, the samples were briefly washed with tap water on a 63-μm sieve in order to remove organic particles from the surface of the foraminiferal tests and to break up aggregations of material. Due to the very high concentration of LPF in June, the samples were split by a Motodo plankton sample divider. The number of specimens in resulting aliquots was used to calculate the total concentration of foraminifera in the sample. The foraminifera were manually counted and identified to species level under a Leica MZ12.5 light microscope following the taxonomy of Schiebel and Hemleben (2017) and SCOR WG 138 (http://www.eforams.org/index.php/WG138_Taxonomy).

3.4. Planktonic Foraminifera From Surface Sediment

In order to retrieve recently dead adult specimens from the surface sediments, a box-corer (50 × 50 × 50 cm) was deployed from the ship. Immediately after recovering the sediment core, the top layer (1 cm) was scraped off by a spoon, and preserved in approximately 50 ml of ethanol (96%) with rose bengal (2 g L^{-1} of ethanol), and stored at 2 °C. In the home laboratory, the samples were sieved through a 63-μm sieve and dried for at least 24 hr at 40 °C. Once dried, planktonic foraminifera were picked under a light microscope, with a fine brush, and identified to species level.

3.5. Planktonic Foraminifera and *Limacina helicina* Morphometrical Parameters

For size measurements, the LPF and *L. helicina* from the water column, in addition to planktonic foraminifera from surface sediments, were uniformly arranged on a slide with the umbilical side facing upward. Images were acquired by a Leica Z16 APO microscope, using the integrated Leica DFC450 camera and LAS version 4.12.0 software. The images were processed using the ruler tool in Adobe Photoshop CS6, with

which the minimum and maximum diameters that bisect the center of the foraminiferal tests were measured in microns always by the same operator to be as accurate as possible.

3.6. Stable Isotopes

Stable isotopes of carbon and oxygen from LPF shells were analyzed at The Stable Isotope Laboratory at CAGE—Centre for Arctic Gas Hydrate, Environment and Climate located at UiT—The Arctic University of Norway, Tromsø, Norway. Due to the low concentration and dominance of small shells in April, stable isotope analysis was only performed on the LPF from June. Twenty specimens of *Neogloboquadrina pachyderma* and 20 specimens of *Turborotalita quinqueloba* of the same size class (150–200 μm) were picked from all five sampling depths and placed in 4.5 ml vials. A total of 20 samples were analyzed, 10 for each species. The vials were flushed with He, and five drops of water-free H_3PO_4 were added manually with a syringe. After equilibration for more than 3 hr at 50 °C, the samples were analyzed on a Gasbench II and Thermo Scientific MAT253 IRMS. Isotopic values are reported vs. the VPDB scale, which has been normalized by two to three inhouse standards with a wide range of $\delta^{13}C$ and $\delta^{18}O$ values. The inhouse standards have been normalized by several international standards. Instrument uncertainty of $\delta^{13}C$ and $\delta^{18}O$ is standard deviation ≤0.1‰ (ThermoScientific).

3.7. Statistical Analyses

To test for difference between the environmental parameters sampled in the surface and bottom waters of April and June, a Mann-Whitney *U* test (Mann & Whitney, 1947) was conducted on the data. The stations were separated into their surface (0–100 m) and bottom (100–300 m) water samples.

To test for possible significant differences between the LPF population sampled in April and June, we used a Mann and Whitney *U* test and tried the following hypothesis:

1. Are LPF concentrations (all species together) and test size significantly different between sampling periods?
2. Are specific (species by species) LPF concentrations significantly different between sampling periods?
3. Are LPF concentrations by depth significantly different between sampling periods?
4. Which environmental parameters are significantly different between the sampling periods?

To determine if there is a relationship between the maximum CH_4 concentration at each station and LPF concentration in the overlying water column, and primary production indicators, we performed a Pearson's correlation test on both April and June data. Both the Pearson's correlation tests and the Mann-Whitney *U* tests were performed on the program RStudio (Version 1.2.1335) (RStudio Team: RStudio: Integrated development for R, 2015). In order to compare the species diversity within the LPF population between April and June, the Shannon Index (*H′*) (Shannon & Weaver, 1949) was calculated.

4. Results

4.1. Environmental Parameters

Temperature and salinity, the CO_2 system parameters (DIC, A_T, pH, and calcium carbonate saturation states Ω), and primary production indicators along the 9-km transect reveal clear seasonal differences between April and June. In April, the water column is well mixed in terms of temperature and salinity (Figures 2a and 2b), with temperature ranging between 2.77 °C and 3.77 °C, and the salinity between 34.99 and 35.02. In April, the water column is dominated by AW with an occasional presence of TAW in the bottom ~50 m. In June, the temperature ranges from 2.1–7.03 °C, increasing toward the surface, and the salinity between 35 and 35.02. In June, the water column is more thermally stratified, with a surface mixed layer extending to ~50 m water depth. In June, the lower ~100 m of the water column is dominated by the colder TAW, and the upper ~250 m is dominated by AW. Sea surface temperature increased by 3.26 °C from April to June, while the salinity remained almost constant. This allows for the investigation of seasonal changes in thermal stratification on the LPF and *Limacina helicina*. In Figures 2 and 3, all parameters are presented on the same scale, with the exception of CH_4, due to the large difference in concentration between the two sampling seasons (Figures 2c and 3c).

In April (Figure 2), our data show two CH_4 plumes close to the seafloor (Figure 2c), which also correspond to plumes of elevated DIC and fCO_2 (Figures 2d and 2k). These plumes of elevated CH_4 and carbon originate

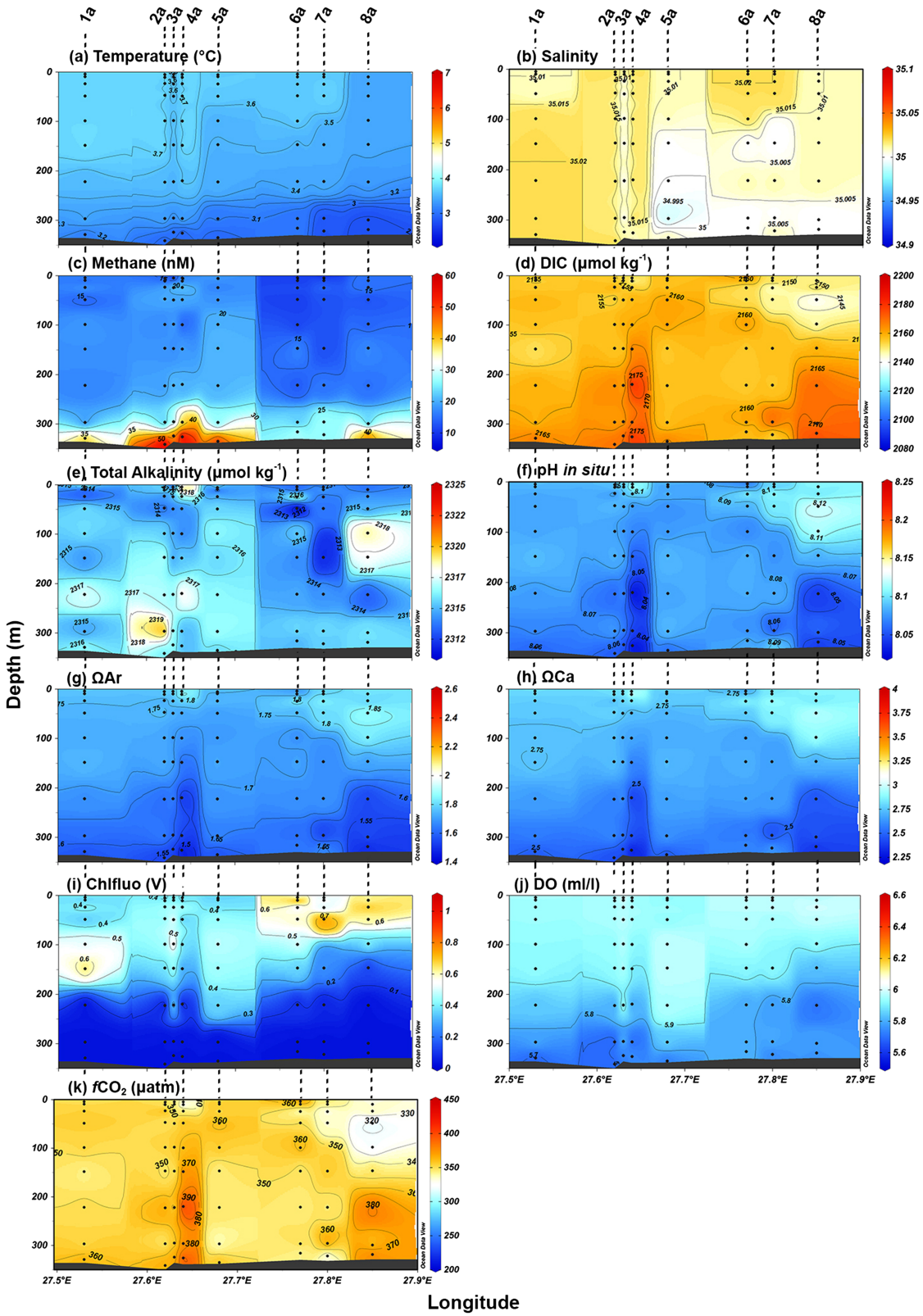

Figure 2. Vertical sections of (a) temperature (°C), (b) salinity, (c) methane (nM), (d) dissolved inorganic carbon (DIC, µmol kg^{-1}), (e) total alkalinity (A_T, µmol kg^{-1}), (f) pH, (g) aragonite saturation (Ω_{Ar}), (h) calcite saturation (Ω_{Ca}), (i) chlorophyll *a*-fluorescence (chlfluo, V), (j) dissolved oxygen (DO, ml L^{-1}), and (k) carbon dioxide fugacity (fCO_2, µatm) in April 2016. Black dots represent sampling depth for water samples throughout the water column. Station IDs are given on the top of the figure.

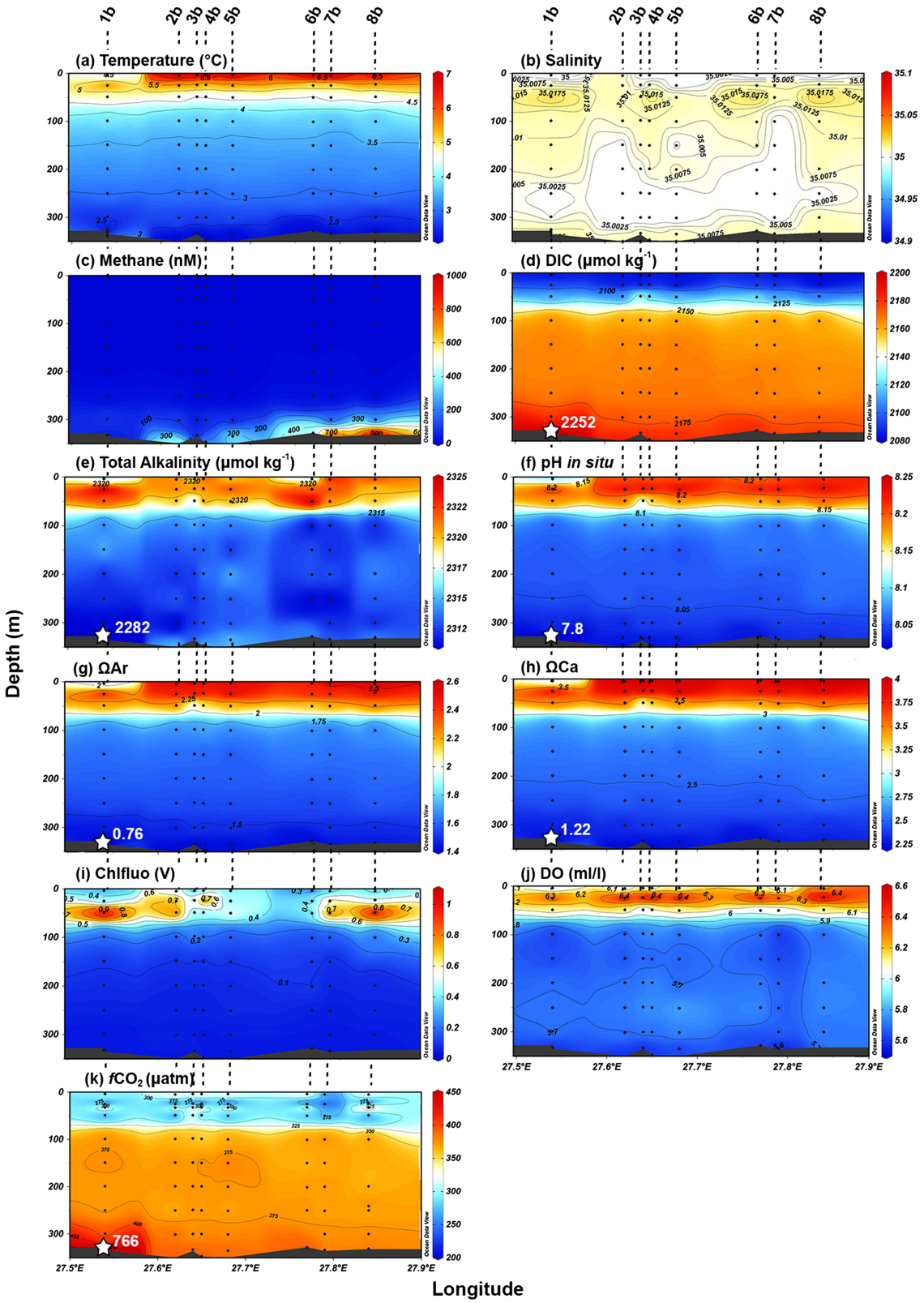

Figure 3. Vertical sections of (a) temperature (°C), (b) salinity, (c) methane (nM), (d) dissolved inorganic carbon (DIC, µmol kg^{-1}), (e) total alkalinity (A_T, µmol kg^{-1}), (f) pH, (g) aragonite saturation (Ω_{Ar}), (h) calcite saturation (Ω_{Ca}), (i) chlorophyll *a*-fluorescence (chlfluo, V), (j) dissolved oxygen (DO, ml L^{-1}), and (k) carbon dioxide fugacity (fCO_2, µatm) in June 2016. Black dots represent sampling depth for water samples throughout the water column. White stars and white text are concentrations from bladecore samples at sediment-water interface. Station IDs are given on the top of the figure.

from the seafloor at 27.65 and 27.85°E and extend upward to approximately 200 m water depth. The maximum CH_4 concentration is 57 nM, found at stations 2a and 4a, at 13 and 9 m above the seafloor, respectively (Figure 2c). The CH_4 concentration is elevated throughout the entire water column (average concentration = 15.7 nM), with only a slight gradient from the seafloor to the surface. From 300 m water depth to the seafloor, the average CH_4 concentration reaches 31.8 nM. The CH_4 concentration decreases from 300 to 5 m water depth to reach 15.7 nM. The plumes are also characterized by lower pH, Ω_{Ar}, and Ω_{Ca} (pH = 8.02, Ω_{Ar} = 1.4, Ω_{Ca} = 2.3), compared to surrounding waters (pH = 8.08, Ω_{Ar} = 1.7, Ω_{Ca} = 2.7). A_T is slightly elevated at the plume locations, and ranges from 2,311 to 2,321 μmol kg^{-1}.

In June, the CH_4 concentrations close to the seafloor are on average more than one order of magnitude higher than in April, with a maximum concentration of 959 nM at station 8b, 1 m above the seafloor (Figure 3c). Elevated CH_4 concentrations extend to 150 m, shallower than in April (200 m). From 300 m water depth to the seafloor, the average CH_4 concentration is 275 nM, and from 300 to 5 m water depth it is 9.3 nM. Waters at the seafloor were recorded to have Ω_{Ar} as low as 0.76 at station 1b, this coincides with relatively low temperature (2.5 °C), high DIC (2,252 μmol kg^{-1}) and a pH of 7.8 (Figure 3g). The fCO_2 in the waters at the seafloor at station 1b is 766 μatm (Figure 2k). The A_T is elevated at the top 75 m (TA > 2,318 μmol kg^{-1}) compared to the rest of the water column (Figure 3e). In the upper 75 m of the water column, DIC values decreased from about 2,160 μmol kg^{-1} in April (Figure 2d), to <2,100 μmol kg^{-1} in June (Figure 3d), coinciding with increased A_T, pH, DO, and chlfluo (Figures 3e, 3f, 3i, and 3j). The surface DO and chlfluo are higher in June than in April (DO: 5.8 to 6.5 ml L^{-1} vs. 5.9 to 6 ml L^{-1}, chlfluo: 0.3 to 1 ml L^{-1} vs. 0.5 to 0.7 ml L^{-1}), suggesting higher primary production in June relative to April. In the layer between 100 and 250 m water depth, the CO_2 system parameters (DIC, A_T, pH, Ω) are relatively homogenous.

Overall, from April to June we observe a thermal stratification of the water column and an increase in CH_4 concentration with increasing water depth. Although the seafloor CH_4 concentrations were higher in June compared to April, its global background concentration along the sampled transect was higher in April. The DIC concentrations in the waters at the seafloor increased from April to June and high values of about 2,200 μmol kg^{-1} encompassed the entire study area.

4.2. Microbial Methane Oxidation Activity

The highest microbial methane oxidation activity is found close to the seafloor (0–15 m above seafloor) with a maximum value of 32 nM d^{-1} at station M10 (Figure 4, Table S6). The average MO_X activity close to the seafloor from all stations along the transect is 11 nM d^{-1}. At the sea surface and in the water column down to 215 m, MO_X activity was below detection limit. Methane concentrations are highest in the bottom waters (0–25 m above sea floor), and range from 38 (station M8) to 767 nM (Station M5).

4.3. Planktonic Foraminiferal Concentrations and Assemblages in the Water Column and Surface Sediments

In April, LPF concentrations are low, ranging from 0 (station 7a, 200–300 m depth) to 6 (station 1a, 0–50 m depth) individuals (ind.) m^{-3} (Figure 5). Also in April, benthic foraminifera occur in the Multinet samples at all of the stations with the exception of 7a. In June, the concentration of planktonic foraminifera is higher compared to April, and ranges from 12 ind. m^{-3} (station 8b, 200–300 m depth) to 436 ind. m^{-3} (station 2b, 50–100 m depth) (Figure 5). In June, benthic foraminifera are only found in the Multinet samples from station 8b. Maximum concentrations of LPF in both seasons are located in surface waters (0–100 m), and the lowest in the 100–300 m water depth interval. The total concentrations of LPF across all stations is 87 ind. m^{-3} in April, and 4,637 ind. m^{-3} in June, with an average per station of 11 and 580 ind. m^{-3}, respectively. During both seasons, the five stations to the west (1a/b, 2a/b, 3a/b, 4a/b, 5a/b; Figures 1b and 6) have a higher concentration of LPF compared to the three stations to the east (6a/b, 7a/b, 8a/b) (Figure 5). The concentration of LPF along the 9-km transect is highly variable both in April and June (Figure 6).

There are seven LPF species present in April and 12 in June (Figure 7). The assemblages of April and June are both largely dominated by *Turborotalita quinqueloba* and *Neogloboquadrina pachyderma*, where they together make up to 90.6% and 88.8% of the total LPF community, respectively. This allows for a comparison

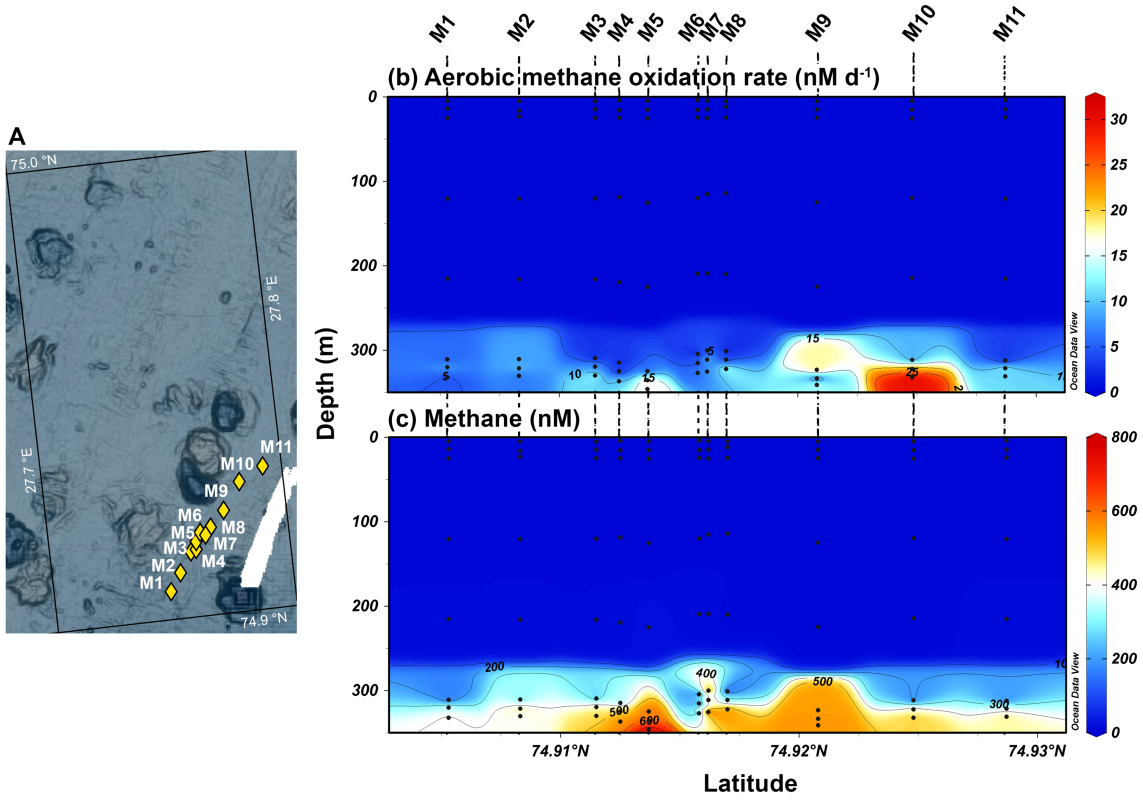

Figure 4. (a) Map over MO_X and methane sampling stations, and vertical sections of (b) aerobic methane oxidation rate (nM d^{-1}) and (c) methane (nM).

of the size distribution of the *T. quinqueloba* and *N. pachyderma* that were present in April and June (Figure 9).

At most stations and during both sampling periods *T. quinqueloba* is the dominant species reaching maximum concentrations in April and June of 6 and 355 ind. m^{-3}, respectively. In April *T. quinqueloba* makes up 77.7% of the community, while *N. pachyderma* makes up 12.9%. In June, *T. quinqueloba* makes up 64.3%, while *N. pachyderma* makes up 24.5% (Figure 7). Two significant differences are the decrease of *Neogloboquadrina incompta* percentages from 5.2% in April to 0.9% in June. The other significant difference between spring and summer is the increase in the *Globigerinita uvula* population from 2.5% to 6.6%. The June LPF community is more diverse ($H' = 1.12$ vs. 0.81), and includes specimens of *Globigerina bulloides*, *Orcadia riedeli*, *Turborotalita humilis*, and *Globigerinoides conglobatus*. None of the LPF specimens from the surface sediments were stained. *Turborotalita quinqueloba* is the most dominant species in the surface sediments, making up 80% of the fauna, while *N. pachyderma* and *G. uvula* make up 16% and 4%, respectively (Figure 7c).

4.4. *Limacina helicina* Concentrations

Limacina helicina is the only pteropod species found in our samples from the crater area. Similar to the LPF, *L. helicina* specimens are more abundant in summer than in spring, with the highest concentration in the surface waters (0–50 m depth) (Figure 8). However, the increase in overall concentration across all stations from 41 to 127 ind. m^{-3} is not as dramatic compared to the LPF community (37 to 1,971 ind. m^{-3}). During both periods, *L. helicina* was absent from some samples. In April, the highest concentration at a single station reaches five ind. m^{-3} (station 1a, 0–50 m depth), while in June it is 10 times higher, reaching 47 ind. m^{-3} (station 2b, 0–50 m depth). The concentration in the 100–300 m depth interval does not change much between the two sampling periods. In April, the average concentration in the 100–300 m depth interval is three ind. m^{-3}, while in June it is two ind. m^{-3}. The spring vertical distribution of *L. helicina* is quite

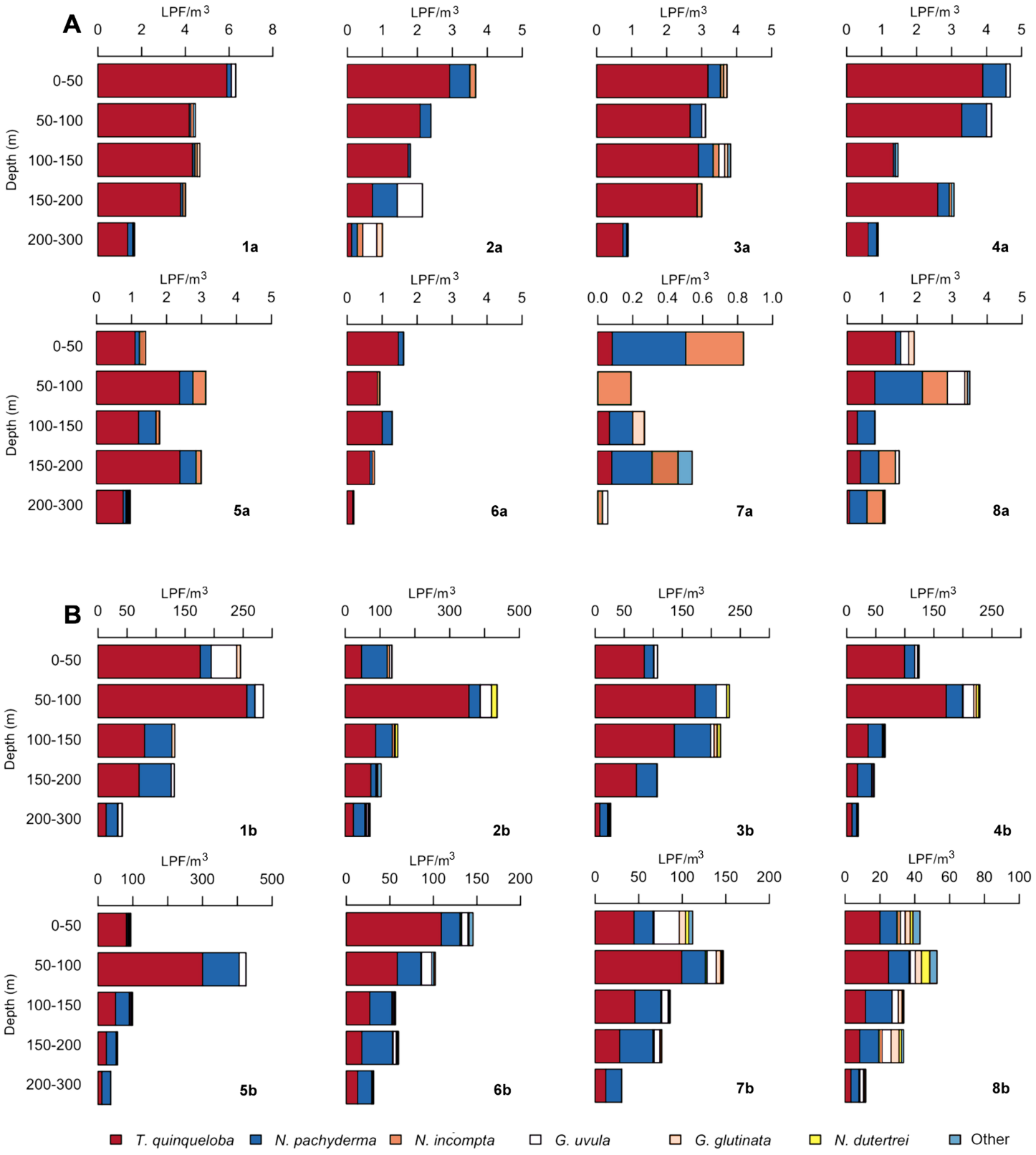

Figure 5. Planktonic foraminiferal abundances (individual (ind.) m^{-3}) per species plotted against water depth (m) for every station sampled in (a) April and (b) June. Bold numbers at the lower right of each graph are station IDs. Please note different *x* axes.

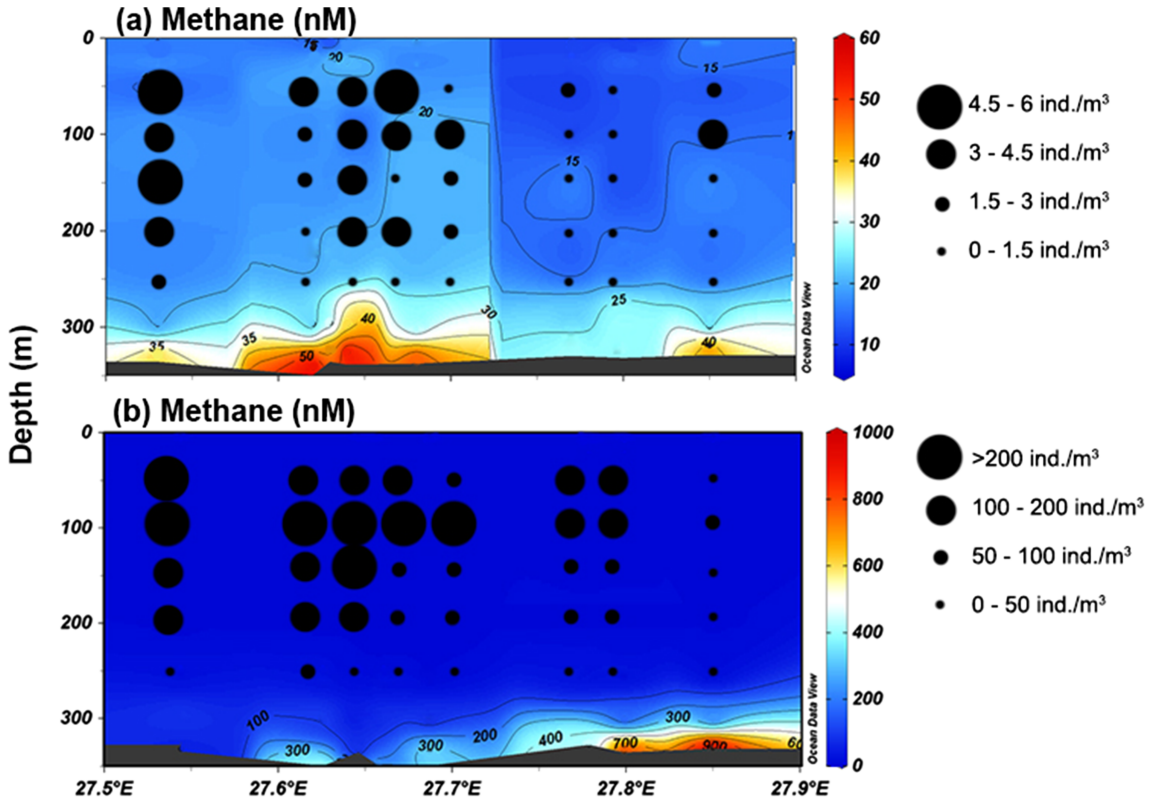

Figure 6. LPF concentration in the water column overlain on methane concentrations for (a) April and (b) June. Note different scales for both methane and LPF concentration. Station IDs are given on top of each cross section.

homogeneous in the depth interval 0–200 m, while in summer the distribution is characterized by a peak in the surface waters (0–50 m) followed by a sharp decline with depth.

4.5. LPF Size Parameters

A total of 1,562 LPF were measured for their diameters, in addition to 56 planktonic foraminifera from surface sediment samples. In April, the test sizes of the LPF assemblages has a mean of 103.3 μm, and are constrained to diameters of 60–200 μm, with the highest frequency of specimens falling in the 100 to 110 μm bin suggesting the community to be largely dominated by small specimens, likely to be juveniles or young adults (Figure 9a). In June, the test sizes have a mean diameter of 188.6 μm and display a larger range with no obvious peak in frequency. The size distribution of June ranges from 80–340 μm (Figure 9a). The June

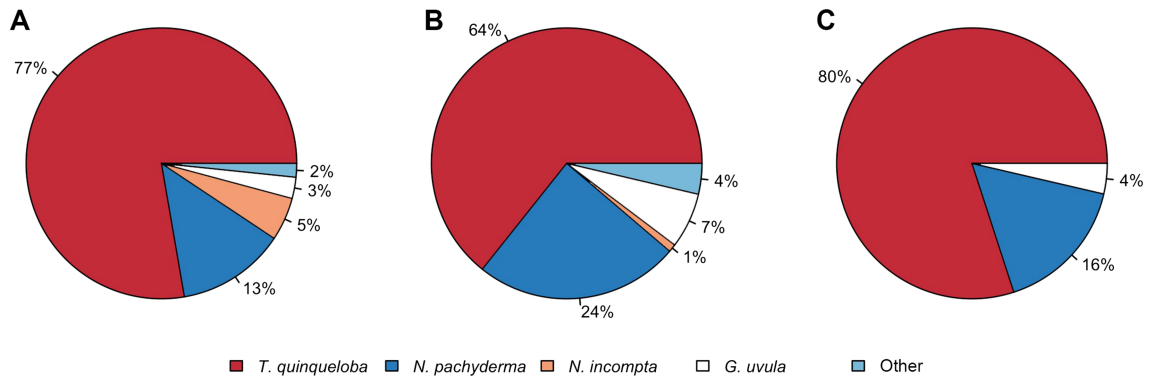

Figure 7. Average LPF species composition across all stations, in (a) April, (b) June, and in (c) surface sediments in the crater area.

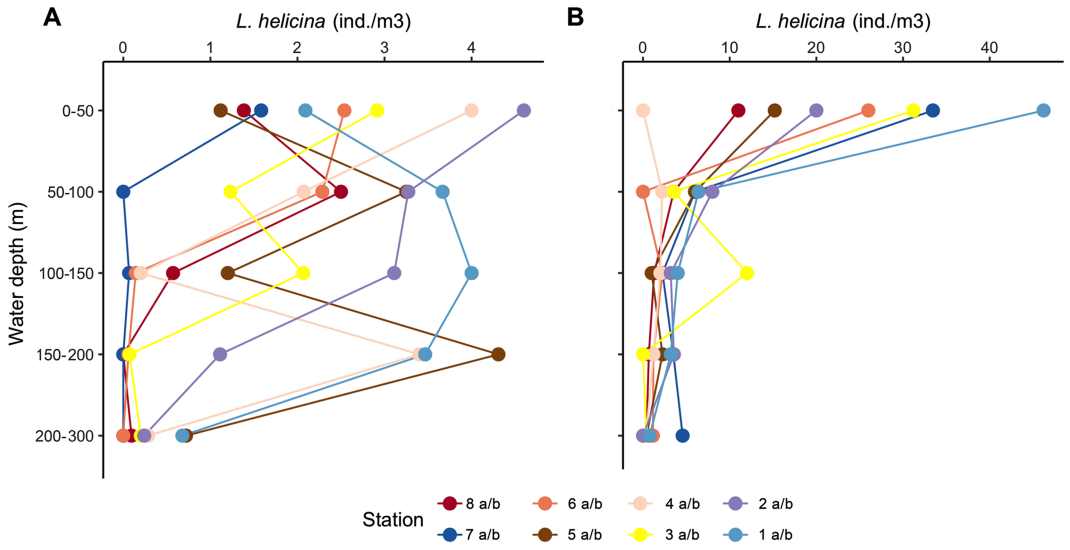

Figure 8. Vertical concentration of *Limacina helicina* (individuals (ind.) m^{-3}) for stations sampled in (a) April and (b) June. Note different scales of *x* axes.

population consists of a mix between small and large specimens, likely to be both adults and juveniles. The recently dead population in the surface sediments has a size distribution of 100–330 μm, with the highest frequency of specimens falling in the 210 to 220 μm bin and in the 230 to 240 μm bin (Figure 9a). The diameters of *N. pachyderma* and *T. quinqueloba* were not found to be significantly different ($p = 0.68$), therefore the increase in LPF diameter from April to June is not a reflection of the increase in the relative concentration of *N. pachyderma* (13% to 24% of the LPF community).

In April, the largest tests are found in the 200–300 m water depth interval, where the average test diameter is 107.95 μm. The smallest tests were in the 0–50 m interval, with an average diameter of 98.85 μm (Figure 9c). In June, the largest tests are in the 150–200 m water depth interval, where the average test diameter is 210.77 μm. The smallest tests are found within the 200–300 m water depth interval, with an average diameter of 157.1 μm (Figure 9d). The difference in test size between April and June at the crater area is statistically significant (Figure 9e).

Seven LPF shell diameters in April ($n = 957$) were found to be smaller than 64 μm, the mesh size of the nets, and none in June ($n = 605$).

4.6. *Limacina helicina* Size Parameters

The shell diameter of 331 specimens of *L. helicina* was measured (256 from April and 175 from June). In April, the shell diameters are constrained to 150–300 μm, with the most frequent diameter falling in the 150 to 200 μm bin. As in the LPF population small specimens, in this case, veliger larvae, are dominant. In June, the size distribution widens, ranging from 150–1200 μm with no clear dominant size frequency. The seasonal size trend of *L. helicina* mirrors that of the LPF population, in that the April population is largely dominated by small specimens, likely to be juveniles or young adults, and the June population consists of a mix between small and large specimens, likely to be both adults and juveniles.

4.7. Stable Isotopes of LPF

In June, the $\delta^{18}O$ composition of *N. pachyderma* in the water column ranges from 2.3‰ to 3.17‰ (Figure 10a; Table S2). The highest $\delta^{18}O$ value is found in the 200–300 m depth interval at station 8b, and the lowest in the 0–50 m interval at stations 8b and 5b. For *T. quinqueloba*, the $\delta^{18}O$ values range from 1.82‰ to 2.74‰ (Figure 10a; Table S2). The highest $\delta^{18}O$ value is found in the 100–150 m depth interval at station 5b, and the lowest in the 0–50 m interval at station 8b. For both species, a general trend of decreasing $\delta^{18}O$ values with shallower water depth is shown by the linear regression line. The linear regressions for *N. pachyderma* and *T. quinqueloba* have r^2 values of 0.44 and 0.13, respectively.

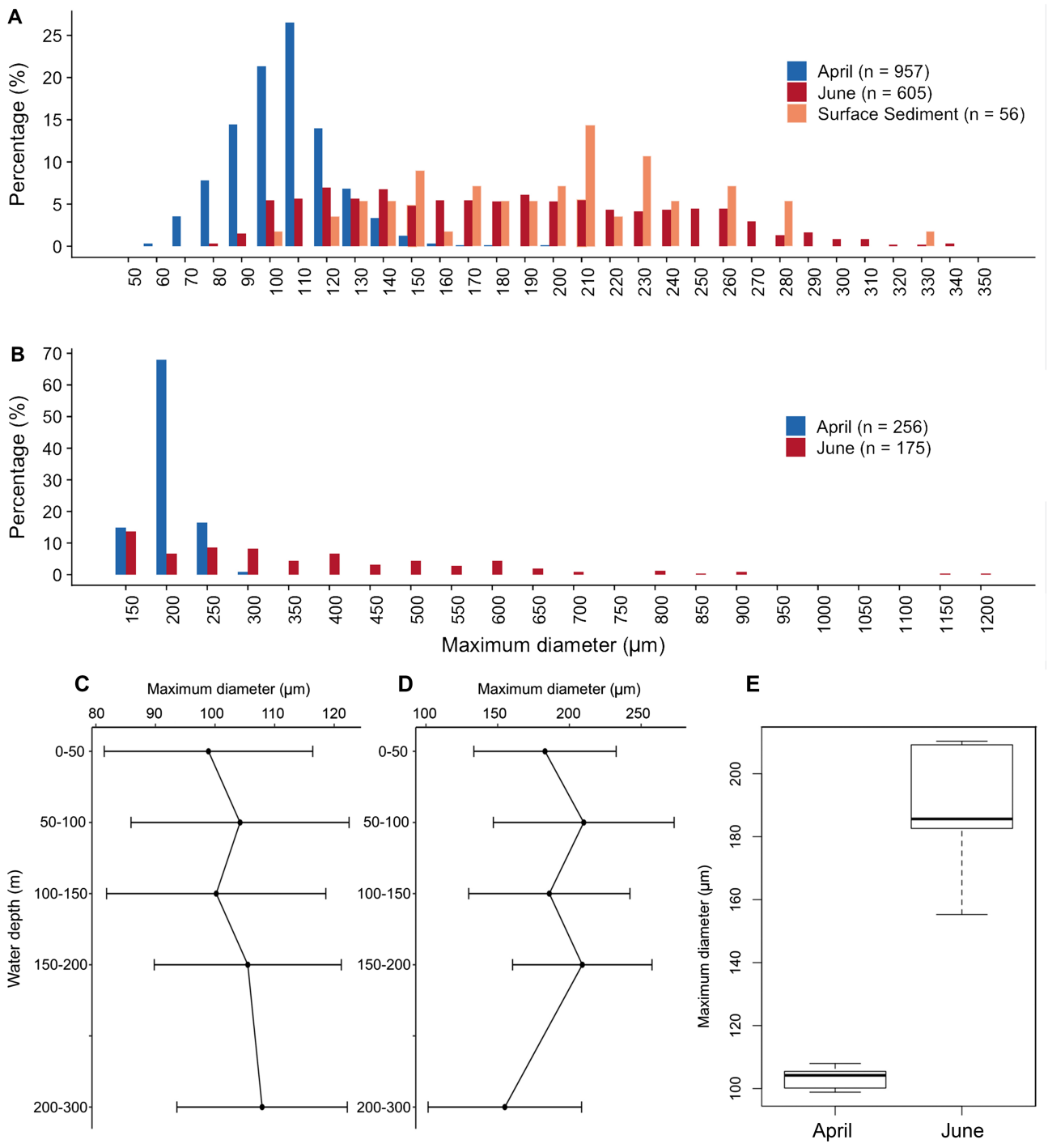

Figure 9. Size distribution of (a) LPF and planktonic foraminifera from surface sediments and (b) *Limacina helicina* in the crater area in April (blue) and June (red). Note different scales of *y* axes. Vertical distribution of LPF test sizes in the crater area in (c) April and (d) June, in addition to standard deviation, and (e) a box-and-whisker plot of test size. Note different scales of *x* axes.

The $\delta^{13}C$ composition of *N. pachyderma* in the water column ranges from −1.02‰ to −0.17‰ (Figure 10b, Table S2). The highest $\delta^{13}C$ value is found in the 200–300 m depth interval at station 5b, and the lowest $\delta^{13}C$ value is found in the 50–100 m interval at stations 8b. For *T. quinqueloba*, the $\delta^{13}C$ values ranged from −2.39‰ to −1.1‰ (Figure 10b, Table S2). The highest value was found in the 100–150 m depth interval at station 5b, and the lowest in the 0–50 m interval at station 8b. The linear regression line for *N.*

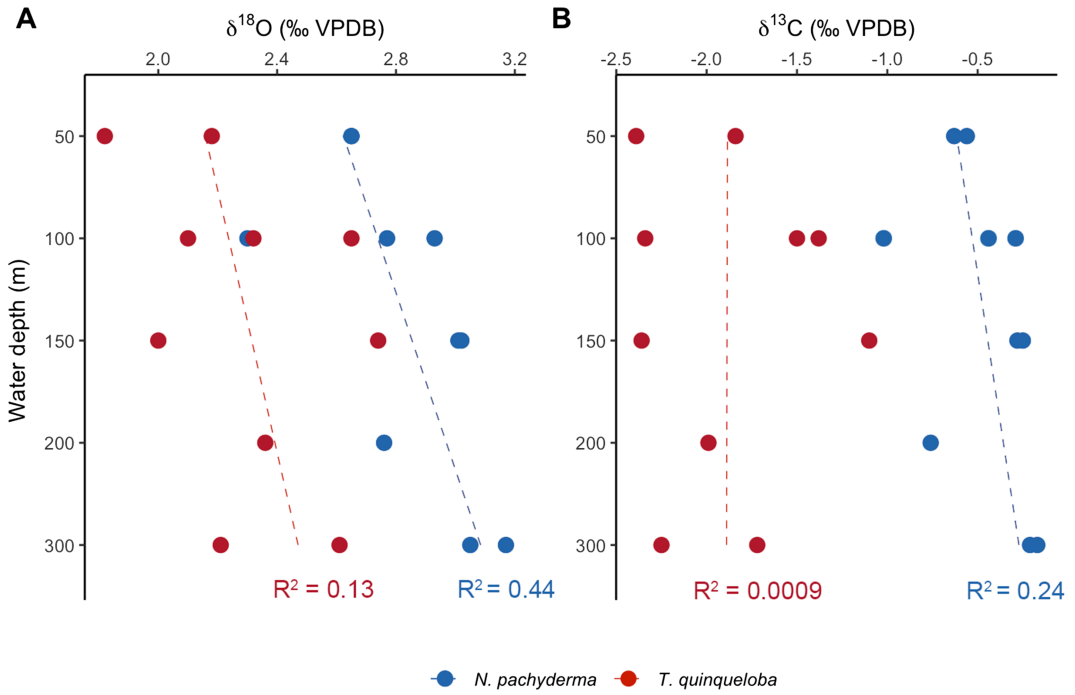

Figure 10. (a) $\delta^{18}O$ and (b) $\delta^{13}C$ values of *Neogloboquadrina pachyderma* (blue) and *Turborotalita quinqueloba* (red) in June. Dashed line indicates the linear regression for the respective species.

pachyderma shows a general trend of increasing $\delta^{13}C$ values with depth, and an r^2 value of 0.24. The $\delta^{13}C$ values of *T. quinqueloba* throughout the water column do not show any trend.

4.8. Statistical Analyses

All environmental parameters in the surface (0–100 m) and bottom (100–300 m) waters show a statistically significant difference between the two sampling periods, with the exception of surface water chlfluo (p = 0.22) (Table S3). All LPF variables, that is, total concentration, concentration by depth, species-specific concentrations, and test sizes, also show statistically significant differences between the two sampling seasons (Table S4). The Shannon diversity index (H') for the LPF community in spring is 0.81, while in summer, it is 1.12. During both seasons, there is no statistically significant correlation between CH_4 concentration and overlying LPF concentration, chlfluo or DO (Table S5).

5. Discussion

There are 47 planktonic foraminiferal morphospecies in the modern ocean (SCOR WG 138), but few can be found in any considerable numbers in the Arctic and polar regions. The Arctic and northern polar LPF population shows a low diversity, and is dominated by *Neogloboquadrina pachyderma* and *Turborotalita quinqueloba* (e.g., Carstens et al., 1997; Eynaud, 2011; Jensen, 1998; Pados & Spielhagen, 2014; Volkmann, 2000), similar to our samples from the Barents Sea. In addition, our samples from April and June in the crater area highlight the highly heterogeneous nature of the LPF spatial distribution (Meilland et al., 2019) along the 9 km transect (Figure 6). It has been shown that the zooplankton community in the Barents Sea display strong seasonal variability in terms of their concentration and community composition (Arashkevich et al., 2002). This seasonality is caused by variations in sea surface temperature and phytoplankton biomass. The phytoplankton biomass at a given site is controlled by changes in the mixed layer depth, brought on by thermal stratification. The shoaling of the mixed layer depth enables nutrient pumping (e.g., Bé, 1960) and creates an environment with high nutrient and light levels, marking the start of the phytoplankton bloom. Wind driven mixing supplies nutrients and supports a prolonged primary production into summer and early fall. It has been found that in cold regions, primary productivity serves as a timing cue for when conditions are

suitable for growth and reproduction of the LPF (Kretschmer et al., 2016). Typically, the highest concentrations of LPF occurs during the summer (e.g., Fischer et al., 1988; Kretschmer et al., 2016).

In addition to the potential shift in LPF phenology, a change in the LPF faunal composition at high latitude regions, as a result of ocean warming, has already been observed. For example, the species diversity has increased over the past few decades. There is a higher concentration of the subarctic species *Orcadia riedeli*, *Globigerinita uvula*, and *Neogloboquadrina incompta* (Meilland, 2015; Meilland et al., 2018) in polar regions compared to preindustrial times (Jonkers et al., 2019) (Figures 5 and 7). The observed recent increase in LPF diversity highlights that the Arctic and polar LPF community is changing. Our study shows the current composition of the LPF population in the northern Barents Sea, and its seasonal (spring to summer) development in relation to changes in the environmental conditions, including CH_4, in the water column.

5.1. LPF Seasonal Variability

We observe significant differences in the LPF community sampled in the Barents Sea crater area between April and June (Table S4) and in all the environmental parameters (Table S3), with salinity being the least variable and surface CH_4 being the most (Figures 2b, 2c, 3b, and 3c). Seasonal variations in plankton communities and water properties in the Barents Sea have been intensely studied (e.g., Arashkevich et al., 2002; Loeng et al., 1997; Oziel et al., 2016; Oziel et al., 2017; Reigstad et al., 2002; Wassmann & Slagstad, 1993). March represents the winter season in the central and northern Barents Sea, with very low chlorophyll *a* concentrations in the water column (Reigstad et al., 2002). In the crater area, thermal stratification of the water column starts in April (spring) following the rise in daylight. Although stratification is very subtle in our temperature profile, the two-layered water column (divided at 200 m) can be seen clearly in the chlfluo and DO profiles (Figures 2a, 2i, and 2j). In April, the mean test diameter of the LPF population is 103.3 μm, and 88% of the population has a test equal or smaller than 120 μm. The small test size coincides with low concentration (0–6 ind. m^{-3}). This is likely to be the first population of the spring season. The occurrence of small tests in early spring was also found in the Greenland Sea (Jensen, 1998) and the Fram Strait (Gyldenfeldt et al., 2000). The spring bloom in the Barents Sea typically peaks in May and ends in June when nutrients in the surface water layers are depleted and there is stronger zooplankton grazing by planktivorous organisms like chaetognaths and medusae (Arashkevich et al., 2002; Oziel et al., 2017).

In June, the thermal stratification of the water column in the crater area is much more pronounced and the boundary layer is shallower (at 100 m). Above 100 m water depth, we find the highest concentration of LPF and *Limacina helicina* (Figures 5b and 8). The increase in DO and chlfluo coincide with the thermocline and are indicative of primary production in the surface waters (Figures 3a, 3i, and 3j). Since salinity did not change significantly between April and June in the crater area, the decreased DIC of about 60 μmol kg^{-1} is most likely due to CO_2 uptake during photosynthesis (Figure 3d). The difference in the surface water chlfluo ($p = 0.22$) between April and June is not significant, suggesting that April represents the start of the spring bloom and in June the end of the spring bloom, where nutrients may already be depleted. By June, the water temperature in the crater area has apparently increased sufficiently to include the thermal range tolerated by the nonpolar species *Orcadia riedeli* and *Globigerinoides conglobatus*. The water temperature at the time of sampling represents also the modeled optimal temperature for *N. pachyderma* (Kretschmer et al., 2018). Only 19.9% of the population has a test diameter equal or smaller than 120 μm, meaning that the relative concentration of juveniles has greatly reduced in June, compared to April. In terms of concentrations, we see a 53-fold increase from April to June (43–436 ind. m^{-3}), but there is no dominant size of individuals (test diameter) (Figure 9a), suggesting that we are capturing several cohorts, in contrast to April. Larger tests during times of high flux of LPF are also found in the Fram Strait (Gyldenfeldt et al., 2000). In April, we see an increase in size with depth, while the opposite occurs in June, suggesting that juveniles do not have a preferred habitat depth, or that it is unpredictable.

The seasonal trend in zooplankton biomass is nearly identical to that of the primary productivity (Fulton, 1983), suggesting that zooplankton grazing intensifies simultaneously with increasing phytoplankton productivity. Temperate and cold-water LPF species are characterized by general absence of symbionts, making them reliant on productivity in the water column for food (Jonkers & Kučera, 2015). The changes to the LPF community observed in this study in terms of size and concentration appear to match calanoid copepod seasonality in the same region with spawning of *Calanus finmarchicus* and *Calanus glacialis* in March–April, early adult stages in May, and adult stages in July, which have already started to spawn (Arashkevich

et al., 2002). Our data suggest that *L. helicina* also follows this growth pattern, meaning that LPF and *L. helicina* likely both develop simultaneously with the primary producers (Figure 9b). According to Wang et al. (2017), the life cycle of *L. helicina* comprises two generations per year. The population sampled in April was likely spawned the previous summer and overwintered with minimal to no growth (Figure 9b). By June, the *L. helicina* population had tripled in concentration and increased in test diameter from $\bar{x}$ = 175.6 μm in spring, to $\bar{x}$ = 334.6 μm in summer. It is possible that some of the larger *L. helicina* sampled in April had spawned the summer/fall population sampled in June. The small-sized *L. helicina* we captured in June will then likely spawn in late summer/fall to produce the population that will overwinter.

For the LPF, the Shannon-Wiener Index was higher in June than April (1.12 vs 0.81), reflective of a more diverse community. Overall, we see a close similarity in species composition in the surface sediments compared to the Multinet samples, suggesting that the surface sediments accurately represent the LPF fauna in the overlying water column (Figure 7). Planktonic foraminifera in surface sediments can be biased toward large and fast sinking tests (e.g., Berelson, 2002), which could lead to a misrepresentation of the LPF size composition; however, this does not seem to be the case in our study.

Oziel et al. (2017) recorded that a smaller summer bloom in the Barents Sea develops in July–August, and peaks in September. By late summer, the breakdown of the vertical stratification due to surface cooling and wind mixing cause renewed nutrient enrichment of the surface waters, meaning that the summer bloom can be sustained as long as the irradiance in the euphotic zone is high enough (Oziel et al., 2017). If our sampling period would have been extended to include the early autumn (September–October), we would expect the test size distribution of both LPF and *L. helicina* to show two peaks. One peak should be at the larger end of the size spectrum, comprising the specimens that will end their lifecycle before winter, and one peak at the smaller end, which are likely the specimens that are preparing to hibernate and that will seed the next year's population. However, a smaller mesh size (<64 μm) would likely be needed to capture the overwintering LPF and *L. helicina* populations. By using a mesh size of 64 μm, we do not have any data on the concentration of LPF smaller than 64 μm. However, our data show the advantage in using a 64-μm mesh as opposed to a 100-μm mesh, which would have resulted in excluding a large part of the small-sized April population (Figure 9a). Many seasonal studies, and consequently, models, are based solely on >125 or >150 μm fraction. Our results would therefore indicate that they provide limited information on the population structure of the planktonic foraminiferal faunas.

5.2. Lunar Cycle

It has been shown that many planktonic foraminiferal species are affected by lunar-phased synchronized reproduction, which is superimposed on seasonal changes in shell flux (e.g., Jonkers et al., 2015). It is conceivable that the population captured in the northern Barents Sea on 19 April probably was spawned during the previous full moon (23 March 2016), since the size distribution strongly suggests that this is a single population (Figure 9a). If they were closely linked to the lunar cycle, the size distribution on 29 June would show two distinct populations, one that spawned after the full moon on 21 May, and one from 20 June (Figure 9a). Juvenile specimens grow rapidly and reach a test size of >100 μm in less than 10 days (Hemleben et al., 1989; Spero & Lea, 1996) making it possible for them to be captured in a 64 μm net 9 days later. They should thus produce a peak in the smaller size frequency. However, the lack of peaks in the test size distribution suggests that these individuals are the result of several spawning events (Figure 9a). The variability we observe in the LPF concentration and size on 29 June does not appear to be linked to the lunar cycle, but rather to seasonality.

5.3. Data Comparison to LPF Seasonality in the Greenland Sea and Irminger Sea

There is limited data on the seasonal distribution of LPF in the northern polar and Arctic regions. Global seasonality models are based largely on two sediment trap studies for polar biogeographic regions: Jensen (1998) with two locations (GS/2, 75°N, 0°E and OG5, 72.38°N, 07.72°W) in the Greenland Sea and Jonkers et al. (2010) in the Irminger Sea (59.25°N, 39.66°W). Due to differences in sampling methods, a direct comparison between our Multinet study from the Barents Sea and the sediment trap fluxes from the Greenland Sea and Irminger Sea is not possible. The sediment trap data reflect planktonic foraminifera that have completed their lifecycle and have sunk into the trap, while our multinet data reflect the living community at all stages of their life cycle. However, the sedimentation of specimens tends to follow the

same spatial trends as plankton net samples (Pados & Spielhagen, 2014), meaning relatively high absolute concentration in the water column will be shown as relatively high fluxes to the sediment trap.

There are two prominent peaks in planktonic foraminiferal concentration in the Irminger Sea during the year. Similar to our data from the crater area, in the Irminger Sea, the first population completes their life-cycle by mid-April, while the peak flux into the sediment trap occurs in May–June, and by late June the flux has greatly decreased. Jonkers et al. (2010) show only a slight difference in foraminiferal shell flux to the sediment traps from mid-April to late June. However, small and light shells that completed their life cycle in April may not sink to the sediment trap depths. Due to the 53-fold increase in the LPF population at the crater area between April and June, we would expect the flux to the seafloor in the crater area to be much higher in summer compared to spring. This suggests that the LPF bloom dynamics in the northern Barents Sea may differ from that of the central Irminger Sea. In the Greenland Sea in OG5, the flux of planktonic foraminifera to the sediment trap starts mid-March, and there are still a very low flux of planktonic foraminifera by late April and restricted to the 63–125 μm size fraction. By late June in the Greenland Sea (OG5), there is an increasing presence of planktonic foraminifera in the 125–250 μm fraction—which is in agreement with our size data (Figure 9a), and the overall flux of planktonic foraminifera has doubled. This doubling of the flux and increase in size in the Greenland Sea (OG5) is likely due to the increased presence of phytoplankton in the summer, similar to what we observe at the crater area (Figure 3i). However, the overall largest peak in flux at OG5 does not occur until August, suggesting that the highest concentration of LPF at OG5 occurs in late summer. Because the time series from the Greenland Sea is from 1991–1992, the current seasonal trend at OG5 of planktonic foraminifera may be more similar to our current observations in the crater area due to ocean warming and the reduction of sea ice in the Greenland Sea. Warmer waters cause LPF populations to peak earlier in the year and to shift northward in the northern hemisphere (Jonkers et al., 2019; Jonkers & Kučera, 2015). The northern-most time series of LPF, at GS/2 in the Greenland Sea, shows a narrow LPF production period, and lower flux. In contrast to the Irminger Sea and OG5, there is no spring bloom. The first planktonic foraminiferal flux to the sediment trap appears in June and consists of tests with diameters that fall evenly within the 63–125 and 125–150 μm fraction, and peaks in September. However, GS/2 is the only site out of the three, which is dominated by *T. quinqueloba*. If we are considering the spring to summer development of the LPF community in terms of concentration and size, our seasonal data seem to be most in line with OG5 from the southern part of the Greenland Sea.

The data from the Barents Sea is also in agreement with the global seasonality model by Jonkers and Kučera (2015). The model shows that in high latitude waters, which have a surface temperature above 5 °C, the peak in the LPF concentration occurs early in the summer, slightly after or at the same time as the maximum chlorophyll *a* concentration, validating the tight link between primary production and LPF seasonality. This suggests that our samples in June represent the peak in LPF concentration.

It must be emphasized that since these sediment trap experiments were done in 1991–1992 and 1994–1995 by Jensen (1998) and in 2003–2006 by Jonkers et al. (2010), there may have been changes in the hydrography and water mass properties due to ocean warming and ice melt, resulting in a different LPF seasonality. There are also strong interannual variations in productivity at any given site. Finally, the location of the three sediment trap experiments and our sampling site in the crater area are all in different oceanographic settings, so we would not expect to see the exact same seasonal trends and species compositions.

5.4. The Effect of Methane on Productivity and LPF Biomass

Methane seep ecosystems are unique, because they host chemosynthesis-based communities resulting in an "oasis effect" on the seafloor, due to enhanced macrofaunal biomass and diversity in comparison to nearby nonseep environments (Åström et al., 2018; Levin, 2005; Levin et al., 2016; Sibuet & Olu, 1998; Sibuet & Olu-Le Roy, 2002; Thomsen et al., 2019). At the crater area, numerous frenulate siboglinid worms, the dominant chemosymbiotrophic megafauna in high latitude seeps, and chemosynthetic bacterial mats are recorded (Sen, Duperron, et al., 2018). The impact of CH_4 seepage on benthic productivity and biomass in the Arctic is clear (Åström et al., 2018, 2019), but an effect on the ecosystem in the overlying water column is unknown. Aggregations of various demersal fish have been found at CH_4 seeps around the world, although the cause of this remains unclear (Åström et al., 2019; Bowden et al., 2013; Grupe et al., 2015; Sellanes et al., 2008; Sen, Aström, et al., 2018). We hypothesize that planktonic organisms may behave in the same manner in that they aggregate above seeps.

The hypothesis that CH_4 seepage enhances primary production and hence biomass in the water column has been discussed previously in the literature (e.g., D'Souza et al., 2016; Pohlman et al., 2017; Rakowski et al., 2015). Enhanced primary production and CO_2 uptake has been reported at a site off the west coast of Spitsbergen, which is also characterized by high CH_4 flux from the seafloor (Pohlman et al., 2017). The mechanism, which causes this enhancement, is, however, unknown. One of the hypotheses is that the physical bubbling of CH_4 gas from the seafloor may cause an upwelling of nutrient rich waters. This mechanism may be present even at depths exceeding 1,000 m, particularly if gas plumes are strong and extend high into the water column (D'souza et al., 2016; Leifer et al., 2009). It is feasible that this upwelling effect of nutrient-rich water, and therefore an enhancement of photosynthetic primary production, also occurs at the crater area where the water depth is only 370 m and intense gas seepage with CH_4 bubble streams up to 200 m height were observed (Andreassen et al., 2017).

In addition to the physical bubbling mechanism, potential chemical pathways that could link CH_4 seepage and photosynthetic primary production exist as well. Further evidence to support the links between CH_4 and planktonic biomass was found in a subterranean estuary ecosystem. It was shown that shrimps were feeding on CH_4-derived carbon (Brankovits et al., 2017). Methane-derived carbon could be added to the water column by two mechanisms; first through bubble stripping, which entails gas exchange of CO_2 from CH_4 bubbles (Vielstädte et al., 2015), and second by CO_2 production as a result of active microbial MO_X (equation (1)). An addition of CO_2 into the water column may lead to an increase in primary production if nutrient levels are sufficient (Engel et al., 2013). The hypothesis that CO_2 is added to the water column by gas exchange from CH_4 bubbles is supported by the elevated DIC and A_T in the CH_4 plumes in April, relative to the surrounding water (Figures 2d and 2e). In April, the pH, Ω_{Ar}, and Ω_{Ca} are lower in the plumes than in the surrounding water, likely due to a net CO_2 addition from the CH_4 plumes (Figures 2f and 2g). In June, the high DIC values in waters just above the seafloor are no longer confined in plumes and has likely been accumulating and dispersing since April (Figure 3d). Since A_T is relatively constant between the seasons, CO_2 has most likely caused the elevated DIC. MO_X data from June (Figure 4c) show 14 times higher rates compared to rates measured at another Arctic CH_4 seepage location at Storfjorden, east of Spitzbergen (Mau et al., 2013). It could therefore be possible that plankton are feeding on carbon sourced from methanotrophic bacteria.

Statistical analyses revealed that the CH_4 concentration in the surface water (0–100 m) in our study area showed a significantly higher variability, compared to the temperature changes between the two sampling periods (Figures 2c and 3c), probably controlled by lateral advection. April shows a nearly four-times higher CH_4 concentration in the surface water (Figure 2c), with an average of 16.3 nM compared to 4.4 nM in June. Furthermore, nearly all multinet samples from April contained benthic foraminifera, which also indicates strong lateral advection and increasing the likelihood that CH_4 could be resuspended in the water column. Higher wind stress and lower temperatures in April may have resulted in stronger currents and well-mixed water masses and consequently a stronger vertical redistribution of CH_4 after its release from the seafloor. This vertical redistribution of CH_4 causes less of a vertical gradient in CH_4 concentration in the water column in April compared to June. Currents also dictate the concentration of methanotrophic bacteria in the water column; the stronger the current, the wider the methanotrophic bacteria community gets spread that lowers the quantity of present methanotrophs per sampling point (Steinle et al., 2015). In June, we see a direct correlation between CH_4 concentration and MO_X activity. It is likely that MO_X activity, as well as the concentration of methanotrophic bacteria, would be lower in April, as we see in the CH_4 distribution pattern.

The LPF concentration at the crater area cannot be explained by the concentration of CH_4 in the water just above seafloor as a result of seepage (Table S5) during both sampling seasons (Figure 6). Similarly, we also do not find a positive correlation between CH_4 and the primary production indicators chlfluo and DO (Table S5). Methane appears to be more confined to the bottom waters in June (Figure 3c), perhaps due to the strong thermal stratification, or the high MO_X rates causing the CH_4 to be utilized before it reaches the upper water column. This could eliminate the possibility of direct contact between CH_4 and the LPF in June. The $\delta^{13}C$ values of *N. pachyderma* and *T. quinqueloba* in the water column in June do not show anomalously negative values, indicating no incorporation of CH_4-derived carbon in their tests. Both $\delta^{13}C$ and $\delta^{18}O$ values of *N. pachyderma* and *T. quinqueloba* are comparable to those reported in the Fram Strait (Pados et al., 2015)

and Nordic Seas (Simstich et al., 2003). However, it has been demonstrated that benthic foraminiferal species do not always record the influence of CH_4 in their tests (Hill et al., 2004). Although our data from the crater area does not suggest a link between CH_4 seepage and LPF concentration, the physical and chemical mechanisms, i.e., upwelling of nutrient-rich wasters by gas flares, or the addition of CO_2 to the surface waters by bubble stripping or MO_X, are all plausible in the crater area.

6. Conclusions

We found significant differences in concentration, species composition, and test size between the LPF and *Limacina helicina* sampled at the beginning (April) and toward the end (June) of the spring bloom. The LPF and *L. helicina* seasonal development follows that of calanoid copepods in the same region. Test size and concentrations of both groups increased from April to June potentially as a response to the thermal stratification and increase in food availability, but without any clear link to the lunar cycle. The observation of smaller specimens of LPF and *L. helicina* in spring also suggests the occurrence of only one population/generation in April, while in June several generations and a larger species diversity are displayed. Seasonal studies on LPF, and consequently, models, are based solely on >125 or >150 μm fraction, as opposed to our data which uses the >64 μm fraction. Our results indicate that they provide limited information on the population structure of the planktonic foraminiferal faunas. Isotopic measurements on LPF shells revealed no direct influence of CH_4 flares on their $\delta^{18}O$ and $\delta^{13}C$ composition. Seepage of CH_4 therefore does not directly influence LPF. We, however, speculate that it could indirectly enhance primary production and therefore an increase in biomass in the overlying water column, either through upwelling of nutrient-rich waters or by the addition of CO_2, owing to gas exchange from CH_4 bubbles or through MO_X activity. We believe that the potential fertilizing effect that CH_4 seepage has on the water column might be significant on a regional scale. Future research focusing on CH_4 seepage in marine environments should investigate the linkages between CH_4 input and its uptake by planktonic organisms through the mapping of trophic interactions. This could help to understand how the species or assemblages may benefit from enhanced CH_4 supply.

Data Set

Total foraminiferal and pteropod counts, species concentrations, and filtered volumes are available on the PANGAEA database (https://doi.pangaea.de/10.1594/PANGAEA.904463). The CTD data are available on Norwegian Marine Data Center (https://doi.org/10.21335/NMDC-225800978).

Competing Interests

The authors declare that there are no competing interests.

Acknowledgments
We are very grateful to the captain and crew of the R/V *Helmer Hanssen*, without whom this work would not have been possible. We thank Helene Hodal Lødemel for analyzing the water samples for the determination of the CO_2 system, and general support. We are grateful to Pär Jansson and Pavel Serov for collecting water samples for methane analysis during CAGE cruise 16-2 and 16-5. Pavel Serov and Matteus Lindgren analyzed methane from the water samples, and Matteus Lindgren also performed the stable isotope measurements at The Stable Isotope Laboratory at CAGE—Centre for Arctic Gas Hydrate, Environment and Climate. We thank Cheshtaa Chitkara for the help in taking photographs of LPF and *L. helicina*. Two anonymous reviewers are thanked for their helpful comments that greatly improved the manuscript. This work was supported by the Centre for Arctic Gas Hydrate, Environment and Climate (CAGE), the Research Council of Norway through its Centres of Excellence scheme (grant 223259), and the Ocean Acidification Flagship research program within the FRAM-High North Research Centre for Climate and the Environment.

References

AMAP: AMAP assessment (2013). Arctic Ocean acidification., 2013.

AMAP: AMAP Assessment (2018). Arctic Ocean Acidification, Arctic Monitoring and Assessment Programme (AMAP), Tromsø, Norway (www.amap.no), Tromsø, Norway., 2018.

Andreassen, K., Hubbard, A., Winsborrow, M. C. M., Patton, H., Vadakkepuliyambatta, S., Plaza-Faverola, A., et al. (2017). Massive blow-out craters formed by hydrate-controlled methane expulsion from the Arctic seafloor. *Science* (80-., *356*(6341), 948–953. https://doi.org/10.1126/science.aal4500

Arashkevich, E., Wassmann, P., Pasternak, A., & Wexels Riser, C. (2002). Seasonal and spatial changes in biomass, structure, and development progress of the zooplankton community in the Barents Sea. *Journal of Marine Systems*, *38*(1–2), 125–145. https://doi.org/10.1016/S0924-7963(02)00173-2

Archer, D., Buffett, B., & Brovkin, V. (2008). Ocean methane hydrates as a slow tipping point in the global carbon cycle. *Proceedings of the National Academy of Sciences*, *106*(49), 2059620601. 10.1073/pnas.0800885105

Arrigo, K. R., & van Dijken, G. L. (2011). Secular trends in Arctic Ocean net primary production. *Journal of Geophysical Research, Oceans*, *116*(C9), 1, C09011–15. https://doi.org/10.1029/2011JC007151

Arrigo, K. R., & van Dijken, G. L. (2015). Continued increases in Arctic Ocean primary production. *Progress in Oceanography*, *136*, 60–70. https://doi.org/10.1016/j.pocean.2015.05.002

Åström, E. K. L., Carroll, M. L., Ambrose, W. G., & Carroll, J. (2016). Arctic cold seeps in marine methane hydrate environments: Impacts on shelf macrobenthic community structure offshore Svalbard. *Marine Ecology Progress Series*, *552*, 1–18. https://doi.org/10.3354/meps11773

Åström, E. K. L., Carroll, M. L., Ambrose, W. G., Sen, A., Silyakova, A., & Carroll, J. L. (2018). Methane cold seeps as biological oases in the high-Arctic deep sea. *Limnology and Oceanography*, *63*(S1), S209–S231. https://doi.org/10.1002/lno.10732

Åström, E. K. L., Carroll, M. L., Sen, A., Niemann, H., Ambrose, W. G., Lehmann, M. F., & Carroll, J. (2019). Chemosynthesis influences food web and community structure in high-Arctic benthos. *Marine Ecology Progress Series*, *629*(October), 19–42. https://doi.org/10.3354/meps13101

Bates, N. R., & Mathis, J. T. (2009). The Arctic Ocean marine carbon cycle: Evaluation of air-sea CO_2 exchanges, ocean acidification impacts and potential feedbacks. *Biogeosciences*, *6*(11), 2433–2459. https://doi.org/10.5194/bg-6-2433-2009

Bé, A. W. H. (1960). Ecology of Recent planktonic foraminifera—Part 2, Bathymetric and seasonal distributions in the Sargasso Sea off Nermuda. *Micropaleontology*, *6*(4), 373–392. https://doi.org/10.2307/1484218

Bednaršek, N., Tarling, G. A., Bakker, D. C. E., Fielding, S., Cohen, A., Kuzirian, A., et al. (2012). Description and quantification of pteropod shell dissolution: A sensitive bioindicator of ocean acidification. *Global Change Biology*, *18*(7), 2378–2388. https://doi.org/10.1111/j.1365-2486.2012.02668.x

Bednarsek, N., Tarling, G. A., Bakker, D. C. E., Fielding, S., & Feely, R. A. (2014). Dissolution dominating calcification process in polar pteropods close to the point of aragonite undersaturation. *PLoS ONE*, *9*(10), e109183. https://doi.org/10.1371/journal.pone.0109183

Berelson, W. M. (2002). Particle settling rates increase with depth in the ocean. *Deep-Sea Research Part II: Topical Studies in Oceanography*, *49*(1-3), 237–251. https://doi.org/10.1016/S0967-0645(01)00102-3

Biastoch, A., Treude, T., Rüpke, L. H., Riebesell, U., Roth, C., Burwicz, E. B., ... Wallmann, K. (2011). Rising Arctic Ocean temperatures cause gas hydrate destabilization and ocean acidification. *Geophysical Research Letters*, *38*(8), 16. https://doi.org/10.1029/2011gl047222

Bijma, J., Erez, J., & Hemleben, C. (1990). Lunar and semi-lunar reproductive cycles in some spinose planktonic foraminifers. *Journal of Foraminiferal Research*, *20*(2), 117–127. https://doi.org/10.2113/gsjfr.20.2.117

Bjørklund, K. R., Kruglikova, S. B., & Anderson, O. R. (2012). Modern incursions of tropical Radiolaria into the Arctic Ocean. *Journal of Micropalaeontology*, *31*(2), 139–158. https://doi.org/10.1144/0262-821X11-030

Boetius, A., & Wenzhöfer, F. (2013). Seafloor oxygen consumption fuelled by methane from cold seeps. *Nature Geoscience*, *6*(9), 725–734. https://doi.org/10.1038/ngeo1926

Bowden, D. A., Rowden, A. A., Thurber, A. R., Baco, A. R., Levin, L. A., & Smith, C. R. (2013). Cold seep epifaunal communities on the Hikurangi Margin, New Zealand: Composition, succession, and vulnerability to human activities. *PLoS ONE*, *8*(10), e76869. https://doi.org/10.1371/journal.pone.0076869

Berndt, C., Feseker, T., Treude, T., Krastel, S., Liebetrau, V., Niemann, H., et al. (2014). Temporal Constraints on Hydrate-Controlled Methane Seepage off Svalbard. *Science*, *343*(6168), 284287. https://doi.org/10.1126/science.1246298

Brankovits, D., Pohlman, J. W., Niemann, H., Leigh, M. B., Leewis, M. C., Becker, K. W., et al. (2017). Methane-and dissolved organic carbon-fueled microbial loop supports a tropical subterranean estuary ecosystem. *Nature Communications*, *8*(1), 1835. https://doi.org/10.1038/s41467-017-01776-x

Caldeira, K., & Wickett, M. (2005). Ocean model predictions of chemistry changes from carbon dioxide emissions to the atmosphere and ocean. *Journal of Geophysical Research, C: Oceans*, *110*(C9), 1, C09S04–12. https://doi.org/10.1029/2004JC002671

Carstens, J., Hebbeln, D., & Wefer, G. (1997). Distribution of planktic foraminifera at the ice margin in the Arctic (Fram Strait). *Marine Micropaleontology*, *29*(3–4), 257–269. https://doi.org/10.1016/S0377-8398(96)00014-X

Comeau, S., Gorsky, G., Jeffree, R., Teyssi, J., Villefranche, D. and Cedex, V.: Impact of ocean acidification on a key Arctic pelagic mollusc. pdf, 1877–1882, 2009.

Cottier, F., Tverberg, V., Inall, M., Svendsen, H., Nilsen, F., & Griffiths, C. (2005). Water mass modification in an Arctic fjord through cross-shelf exchange: The seasonal hydrography of Kongsfjorden, Svalbard. *Journal of Geophysical Research, Oceans*, *110*(C12), 1, C12005–18. https://doi.org/10.1029/2004JC002757

Damm, E., Mackensen, A., Budéus, G., Faber, E., & Hanfland, C. (2005). Pathways of methane in seawater: Plume spreading in an Arctic shelf environment (SW-Spitsbergen). *Continental Shelf Research*, *25*(12–13), 1453–1472. https://doi.org/10.1016/j.csr.2005.03.003

Davis, C. V., Rivest, E. B., Hill, T. M., Gaylord, B., Russell, A. D., & Sanford, E. (2017). Ocean acidification compromises a planktic calcifier with implications for global carbon cycling. *Scientific Reports*, *7*(1), 1–8. https://doi.org/10.1038/s41598-017-01530-9

Dickson, A., & Millero, F. (1987). A comparison of the equilibrium constants for the dissociation of carbonic acid in seawater media. *Deep Sea Research Part A, Oceanographic Research Papers*, *34*(10), 1733–1743.

Dickson, A. G. (1990). Thermodynamics of the dissociation of boric acid in synthetic seawater from 273.15 to 318.15 K. *Deep-Sea Research Part I: Oceanographic Research Papers*, *37*(5), 755–766. https://doi.org/10.1016/0198-0149(90)90004-F

Dickson, A. G., Sabine, C. L. and Christian, J. R.: *Guide to best practices for ocean CO2 measurements*., 2007.

Dieckmann, G. S., Spindler, M., Lange, M. A., Ackley, S. F., & Eicken, H. (1991). Antarctic sea ice: A habitat for the foraminifer Neogloboquadrina pachyderma. *Journal of Foraminiferal Research*, *21*(2), 182–189. https://doi.org/10.2113/gsjfr.21.2.182

Dlugokencky, E. J. & Tans, P. P., (2019). NOAA/ESRL.

D'souza, N. A., Subramaniam, A., Juhl, A. R., Hafez, M., Chekalyuk, A., Phan, S., et al. (2016). Elevated surface chlorophyll associated with natural oil seeps in the Gulf of Mexico. *Nature Geoscience*, *9*(3), 215–218. https://doi.org/10.1038/ngeo2631

Engel, A., Borchard, C., Piontek, J., Schulz, K. G., Riebesell, U., & Bellerby, R. (2013). CO_2 increases 14C primary production in an Arctic plankton community. *Biogeosciences*, *10*(3), 12911308. https://doi.org/10.5194/bg-10-1291-2013

Erez, J., Almogi-Labin, A., & Avraham, S. (1991). On the life history of planktonic foraminifera: Lunar reproduction cycle in Globigerinoides sacculifer (Brady). *Paleoceanography*, *6*(3), 295–306. https://doi.org/10.1029/90PA02731

Eynaud, F. (2011). Planktonic foraminifera in the arctic: Potentials and issues regarding modern and quaternary populations. *IOP Conference Series: Earth and Environmental Science*, *14*(1). https://doi.org/10.1088/1755-1315/14/1/012005

Fischer, G., Fütterer, D., Gersonde, R., Honjo, S., Ostermann, D., & Wefer, G. (1988). Seasonal variability of particle flux in the Weddell Sea and its relation to ice cover. *Nature*, *335*(6189), 426–428. https://doi.org/10.1038/335426a0

Fossheim, M., Primicerio, R., Johannesen, E., Ingvaldsen, R. B., Aschan, M. M., & Dolgov, A. V. (2015). Recent warming leads to a rapid borealization of fish communities in the Arctic. *Nature Climate Change*, *5*(7), 673–677. https://doi.org/10.1038/nclimate2647

Fransson, A., Chierici, M., & Nojiri, Y. (2009). New insights into the spatial variability of the surface water carbon dioxide in varying sea ice conditions in the Arctic Ocean. *Continental Shelf Research*, *29*(10), 1317–1328. https://doi.org/10.1016/j.csr.2009.03.008

Fulton, J. (1983). Seasonal and annual variations of net zooplankton at Ocean Station P, 1959–1980. *Canadian Data Report Fisheries and Aquatic Sciences*, *374*, 65.

Graves, C. A., Steinle, L., Rehder, G., Niemann, H., Connelly, D. P., Lowry, D., et al. (2015). Fluxes and fate of dissolved methane released at the seafloor at the landward limit of the gas hydrate stability zone offshore western Svalbard. *Journal of Geophysical Research, Oceans*, *120*(9), 6185–6201. https://doi.org/10.1002/2015JC011084

Greco, M., Jonkers, L., Kretschmer, K., Bijma, J., & Kucera, M. (2019). Variable habitat depth of the planktonic foraminifera Neogloboquadrina pachyderma in the northern high latitudes explained by sea-ice and chlorophyll concentration. *Biogeosciences Discussions*. https://doi.org/10.5194/bg-2019-79

Grupe, B. M., Krach, M. L., Pasulka, A. L., Maloney, J. M., Levin, L. A., & Frieder, C. A. (2015). Methane seep ecosystem functions and services from a recently discovered southern California seep. *Marine Ecology*, *36*(S1), 91–108. https://doi.org/10.1111/maec.12243

Gyldenfeldt, A.-B. V., Carstens, J., & Meincke, J. (2000). Estimation of the catchment area of a sediment trap by means of current meters and foraminiferal tests. *Deep-Sea Research Part II: Topical Studies in Oceanography*, *47*(9–11), 1701–1717. https://doi.org/10.1016/S0967-0645(00)00004-7

Haine, T. W. N., Curry, B., Gerdes, R., Hansen, E., Karcher, M., Lee, C., et al. (2015). Arctic freshwater export: Status, mechanisms, and prospects. *Global and Planetary Change*, *125*, 13–35. https://doi.org/10.1016/j.gloplacha.2014.11.013

Heinz, P., Sommer, S., Pfannkuche, O., & Hemleben, C. (2005). Living benthic foraminifera in sediments influenced by gas hydrates at the Cascadia convergent margin, NE Pacific. *Marine Ecology Progress Series*, *304*, 77–89. https://doi.org/10.3354/meps304077

Hemleben, C., Spindler, M., & Anderson, O. R. (1989). *Modern planktonic foraminifera*, (1st ed.). New York: Springer-Verlag.

Herguera, J. C., Paull, C. K., Perez, E., Ussler, W., & Peltzer, E. (2014). Limits to the sensitivity of living benthic foraminifera to pore water carbon isotope anomalies in methane vent environments. *Paleoceanography*, *29*(3), 273–289. https://doi.org/10.1177/0091270004269562

Hill, T. M., Kennett, J. P., & Valentine, D. L. (2004). Isotopic evidence for the incorporation of methane-derived carbon into foraminifera from modern methane seeps, Hydrate Ridge, Northeast Pacific. *Geochimica et Cosmochimica Acta*, *68*(22), 4619–4627. https://doi.org/10.1016/j.gca.2004.07.012

IPCC: Climate change (2013). The physical science basis. In T. F. Stocker, D. Qin, G.-K. Plattner, M. Tignor, S. K. Allen, J. Boschung, et al. (Eds.), *Contribution of Working Group I to the Fifth Assessment Report of the Intergovernmental Panel on Climate Change*. (Chapter 8, p. 1535). Cambridge, United Kingdom and New York, NY, USA: Cambridge University Press.

Jensen, S. (1998). Planktische Foraminiferen im Europäischen Nordmeer: Verbreitung und Vertikalfluß sowie ihre Entwicklung während der letzten 15000 Jahre, Berichte Sonderforschungsbereich 313, Univ. Kiel, 75(75), 1–105.

Jonkers, L., Brummer, G. J. A., Peeters, F. J. C., Van Aken, H. M., & De Jong, M. F. (2010). Seasonal stratification, shell flux, and oxygen isotope dynamics of leftcoiling N. pachyderma and T. quinqueloba in the western subpolar North Atlantic. *Paleoceanography*, *25*, PA2204. https://doi.org/10.1029/2009PA001849

Jonkers, L., Hillebrand, H., & Kučera, M. (2019). Global change drives modern plankton communities away from the preindustrial state. *Nature*, *570*(7761), 372–375. https://doi.org/10.1038/s41586-019-1230-3

Jonkers, L. and Kučera, M.: Global analysis of seasonality in the shell flux of extant planktonic Foraminifera, *Biogeosciences*, *12*(7), 2207–2226, doi:https://doi.org/10.5194/bg-12-2207-2015, PA22042015.

Jonkers, L., Reynolds, C. E., Richey, J., & Hall, I. R. (2015). Lunar periodicity in the shell flux of planktonic foraminifera in the Gulf of Mexico. *Biogeosciences*, *12*(10), 3061–3070. https://doi.org/10.5194/bg-12-3061-2015

Kaltin, S., & Anderson, L. G. (2005). Uptake of atmospheric carbon dioxide in Arctic shelf seas: Evaluation of the relative importance of processes that influence pCO2 in water transported over the Bering-Chukchi Sea shelf. *Marine Chemistry*, *94*(1–4), 67–79. https://doi.org/10.1016/j.marchem.2004.07.010

Kretschmer, K., Jonkers, L., Kucera, M., & Schulz, M. (2018). Modeling seasonal and vertical habitats of planktonic foraminifera on a global scale. *Biogeosciences*, *15*(14), 4405–4429. https://doi.org/10.5194/bg-15-4405-2018

Kretschmer, K., Kucera, M., & Schulz, M. (2016). Modeling the distribution and seasonality of Neogloboquadrina pachyderma in the North Atlantic Ocean during Heinrich Stadial 1. *Paleoceanography and Paleoclimatology*, 986–1010. https://doi.org/10.1002/2015PA002819

Kucera, M. (2007). Chapter six planktonic foraminifera as tracers of past oceanic environments. *Developments in Marine Geology*, *1*(07), 213–262. https://doi.org/10.1016/S1572-5480(07)01011-1

Leifer, I., Jeuthe, H., Gjøsund, S. H., & Johansen, V. (2009). Engineered and natural marine seep, bubble-driven buoyancy flows. *Journal of Physical Oceanography*, *39*(12), 3071–3090. https://doi.org/10.1175/2009jpo4135.1

Levin, L. A. (2005). Ecology of cold seep sediments: Interactions of fauna with flow, chemistry and microbes. *Oceanography and Marine Biology: An Annual Review*, *43*, 1–46. https://doi.org/10.1201/9781420037449.ch1

Levin, L. A., Baco, A. R., Bowden, D. A., Colaco, A., Cordes, E. E., Cunha, M. R., et al. (2016). Hydrothermal vents and methane seeps: Rethinking the sphere of influence. *Frontiers in Marine Science*, *3*(May), 1–23. https://doi.org/10.3389/fmars.2016.00072

Lewis, E. & Wallace, D. W. R. (1998). CO2SYS-Program developed for CO2 system calculations, ORNL/CDIAC-105, Carbon Dioxide Inf. Anal. Cent., Oak Ridge Natl. Lab., Oak Ridge, Tenn.

Lischka, S., Büdenbender, J., Boxhammer, T., & Riebesell, U. (2011). Impact of ocean acidification and elevated temperatures on early juveniles of the polar shelled pteropod Limacina helicina: Mortality, shell degradation, and shell growth. *Biogeosciences*, *8*(4), 919–932. https://doi.org/10.5194/bg-8-919-2011

Loeng, H. (1991). Features of the physical oceanographic conditions of the Barents Sea. *Polar Research*, *10*(1), 5–18. https://doi.org/10.1111/j.1751-8369.1991.tb00630.x

Loeng, H., Ozhigin, V., & Ådlandsvik, B. (1997). Water fluxes through the Barents Sea. *ICES Journal of Marine Science*, *54*(3), 310–317. https://doi.org/10.1006/jmsc.1996.0165

Mann, H. B., & Whitney, D. R. (1947). On a test of whether one of two random variables is stochastically larger than the other. *Annals of Mathematical Statistics*, *18*(1), 50–60.

Manno, C., Morata, N., & Bellerby, R. (2012). Effect of ocean acidification and temperature increase on the planktonic foraminifer Neogloboquadrina pachyderma (sinistral). *Polar Biology*, *35*(9), 1311–1319. https://doi.org/10.1007/s00300-012-1174-7

Mau, S., Blees, J., Helmke, E., Niemann, H., & Damm, E. (2013). Vertical distribution of methane oxidation and methanotrophic response to elevated methane concentrations in stratified waters of the Arctic fjord Storfjorden (Svalbard, Norway). *Biogeosciences*, *10*(10), 6267–6268. https://doi.org/10.5194/bg-10-6267-2013

Mau, S., Römer, M., Torres, M. E., Bussmann, I., Pape, T., Damm, E. & Geprägs, P. (2017). Widespread methane seepage along the continental margin off Svalbard—From Bjørnøya to Kongsfjorden, Nat. Publ. Gr., (January), 1–13, doi:https://doi.org/10.1038/srep42997.

Mehrbach, C., Culberson, C. H., Hawley, J. E., & Pytkowicx, R. M. (1973). Measurement of the apparent dissociation constants of carbonic acid in seawater at atmospheric pressure1. *Limnology and Oceanography*, *18*(6), 897–907. https://doi.org/10.4319/lo.1973.18.6.0897

Meilland, J. (2015). Rôle des foraminifères planctoniques dans le cycle du carbone marin des hautes latitudes (Océan Indien Austral), Université d'Angers, 2015. Français.

Meilland, J., Schiebel, R., Sanchez, S., & Howa, H. (2018). Abundances and test weights of living planktic foraminifers across the Southwest Indian Ocean: Implications for carbon fl uxes. *Deep Sea Research Part I*, *131*(March 2017), 27–40. https://doi.org/10.1016/j.dsr.2017.11.004

Meilland, J., Siccha, M., Weinkauf, M. F. G., Jonkers, L., & Morard, R. (2019). Highly replicated sampling reveals no species-specific vertical habitats in diurnal vertical migration but stable planktonic foraminifera. *Journal of Plankton Research*, *00*, 1–15. https://doi.org/10.1093/zoolinnean/zly093

Moy, A. D., Howard, W. R., Bray, S. G., & Trull, T. W. (2009). Reduced calcification in modern Southern Ocean planktonic foraminifera. *Nature Geoscience*, *2*(4), 276–280. https://doi.org/10.1038/ngeo460

Niemann, H., Steinle, L., Blees, J., Bussmann, I., Treude, T., Krause, S., et al. (2015). Toxic effects of lab-grade butyl rubber stoppers on aerobic methane oxidation. *Limnology and Oceanography: Methods*, *13*(1), 40–52. https://doi.org/10.1002/lom3.10005

Orr, J. C., Fabry, V. J., Aumont, O., Bopp, L., Doney, S. C., Feely, R. A., et al. (2005). Anthropogenic ocean acidification over the twenty-first century and its impact on calcifying organisms. *Nature*, *437*(7059), 681–686. https://doi.org/10.1038/nature04095

Oziel, L., Neukermans, G., Ardyna, M., Sirven, J., Ruiz-Pino, D., Gascard, J.-C., et al. (2017). Role for Atlantic inflows and sea ice loss on shifting phytoplankton blooms in the Barents Sea. *Journal of Geophysical Research, Oceans*, *122*, 5121–5139. https://doi.org/10.1002/2016JC012582

Oziel, L., Sirven, J., & Gascard, J. C. (2016). The Barents Sea frontal zones and water masses variability (1980-2011). *Ocean Science*, *12*(1), 169–184. https://doi.org/10.5194/os-12-169-2016

Pados, T., & Spielhagen, R. F. (2014). Species distribution and depth habitat of recent planktic foraminifera in Fram Strait, Arctic Ocean. *Polar Research*, *33*(1), 22483. https://doi.org/10.3402/polar.v33.22483

Pados, T., Spielhagen, R. F., Bauch, D., Meyer, H., & Segl, M. (2015). Oxygen and carbon isotope composition of modern planktic foraminifera and near-surface waters in the Fram Strait (Arctic Ocean)—A case study. *Biogeosciences*, *12*(6), 1733–1752. https://doi.org/10.5194/bg-12-1733-2015

Pierrot, D. E. & Wallace, D. W. R. (2006). MS Excel program developed for CO2 system calculations.

Pisso, I., Myhre, C. L., Platt, S. M., Eckhardt, S., Hermansen, O., Schmidbauer, N., et al. (2016). Constraints on oceanic methane emissions west of Svalbard from atmospheric in situ measurements and Lagrangian transport modeling. *Journal of Geophysical Research – Atmospheres*, *121*(23), 14,188–14,200. https://doi.org/10.1002/2016JD025590

Pohlman, J. W., Greinert, J., Ruppel, C., Silyakova, A., Vielstädte, L., Casso, M., et al. (2017). Enhanced CO 2 uptake at a shallow Arctic Ocean seep field overwhelms the positive warming potential of emitted methane. *Proceedings of the National Academy of Sciences*, *19*, 201618926. https://doi.org/10.1073/pnas.1618926114

Rabe, B., Karcher, M., Schauer, U., Toole, J. M., Krishfield, R. A., Pisarev, S., et al. (2011). An assessment of Arctic Ocean freshwater content changes from the 1990s to the 2006-2008 period. *Deep-Sea Research Part I: Oceanographic Research Papers*, *58*(2), 173–185. https://doi.org/10.1016/j.dsr.2010.12.002

Rakowski, C. V., Magen, C., Bosman, S., Rogers, K. L., Gillies, L. E., Chanton, J. P., & Mason, O. U. (2015). Methane and microbial dynamics in the Gulf of Mexico water column. *Frontiers in Marine Science*, *2*, 1–10. https://doi.org/10.3389/fmars.2015.00069

Rathburn, A. E., Levin, L. A., Held, Z., & Lohmann, K. C. (2000). Benthic foraminifera associated with cold seeps on the northern California margin: Ecology and stableisotopic composition. *Marine Micropaleontology*, *38*, 247–266. https://doi.org/10.1016/S0377-8398(00)00005-0

Rebotim, A., Voelker, A. H. L., Jonkers, L., Waniek, J. J., Meggers, H., Schiebel, R., et al. (2017). Factors controlling the depth habitat of planktonic foraminifera in the subtropical eastern North Atlantic. *Biogeosciences*, *14*(4), 827–859. https://doi.org/10.5194/bg-14-827-2017

Reeburgh, W. S. (2013). Global methane biogeochemistry. In *Treatise Geochemistry*, (Second ed., Vol. 5, pp. 71–94). University of California, Irvine, CA, USA: Elsevier Science. https://doi.org/10.1016/B978-0-08-095975-7.00403-4

Reigstad, M., Wassmann, P., Wexels Riser, C., Øygarden, S., & Rey, F. (2002). Variations in hydrography, nutrients and chlorophyll *a* in the marginal ice-zone and the central Barents Sea. *Journal of Marine Systems*, *38*(1–2), 9–29. https://doi.org/10.1016/S0924-7963(02)00167-7

RStudio Team: RStudio: Integrated development for R (2015). RStudio, Inc.

Ruppel, C. D., & Kessler, J. D. (2017). The interaction of climate change and methane hydrates. *Reviews of Geophysics*, *55*(1), 126–168. https://doi.org/10.1002/2016RG000534

Sapart, C. J., Shakhova, N., Semiletov, I., Jansen, J., Szidat, S., Kosmach, D., … Röckmann, T. (2017). The origin of methane in the East Siberian Arctic Shelf unraveled with triple isotope analysis. *Biogeosciences*, *14*(9), 22832292. https://doi.org/10.5194/bg-14-2283-2017

Schiebel, R. (2002). Planktic foraminiferal sedimentation and the marine calcite budget. *Global Biogeochemical Cycles*, *16*(4), 1065. https://doi.org/10.1029/2001GB001459

Schiebel, R., Bijma, J., & Hemleben, C. (1997). Population dynamics of the planktic foraminifer Globigerina hulloides from the eastern North Atlantic. *Deep-Sea Research Part I: Oceanographic Research Papers*, *44*(9–10), 1701–1713. https://doi.org/10.1016/S0967-0637(97)00036-8

Schiebel, R., & Hemleben, C. (2000). Interannual variability of planktic foraminiferal populations and test flux in the eastern North Atlantic Ocean (JGOFS). *Deep-Sea Research Part II: Topical Studies in Oceanography*, *47*(9–11), 1809–1852. https://doi.org/10.1016/S0967-0645(00)00008-4

Schiebel, R., & Hemleben, C. (2017). *Planktic foraminifers in the modern ocean*. Berlin Heidelberg.: Springer-Verlag.

Sellanes, J., Quiroga, E., & Neira, C. (2008). Megafauna community structure and trophic relationships at the recently discovered Concepción Methane Seep Area, Chile, ~36°S. *ICES Journal of Marine Science*, *65*(7), 1102–1111. https://doi.org/10.1093/icesjms/fsn099

Sen, A., Aström, E. K. L., Hong, W. L., Portnov, A., Waage, M., Serov, P., et al. (2018). Geophysical and geochemical controls on the megafaunal community of a high Arctic cold seep. *Biogeosciences*, *15*(14), 4533–4559. https://doi.org/10.5194/bg-15-4533-2018

Sen, A., Duperron, S., Hourdez, S., Piquet, B., Léger, N., Gebruk, A., et al. (2018). Cryptic frenulates are the dominant chemosymbiotrophic fauna at Arctic and high latitude Atlantic cold seeps. *PLoS ONE*, *13*(12), e0209273. https://doi.org/10.1371/journal.pone.0209273

Sen, A., Himmler, T., Hong, W. L., Chitkara, C., Raymond, W., Ferré, B., et al. (2019). Atypical biological features of a new cold seep site on the Lofoten-Vesterålen continental margin (northern Norway). *Scientific Reports*, 1–14. https://doi.org/10.1038/s41598-018-38070-9

Shakhova, N., Semiletov, I., Salyuk, A., Yusupov, V., Kosmach, D., & Gustafsson, Ö. (2010). Extensive methane venting to the atmosphere from sediments of the East Siberian Arctic Shelf. *Science*, *327*(5970), 1246–1250.

Shannon, C. E., & Weaver, W. (1949). *The mathematical theory of communication*. Urbana.: University of Illinois press.

Sibuet, M., & Olu, K. (1998). Biogeography, biodiversity and fluid dependence of deep-sea cold-seep communities at active and passive margins. *Deep-Sea Research Part II: Topical Studies in Oceanography*, *45*(1–3), 517–567. https://doi.org/10.1016/S0967-0645(97)00074-X

Sibuet, M., & Olu-Le Roy, K. (2002). Cold seep communities on continental margins: Structure and quantitative distribution relative to geological and fluid venting patterns. In G. Wefer, D. Billett, D. Hebbeln, B. B. Jørgensen, M. Schlüter, & T. C. E. van Weering (Eds.), *Ocean Margin Systems*, (pp. 235–251). Berlin, Heidelberg: Springer.

Silyakova, A., Greinert, J., Jansson, P. & Ferré, B. (2015). Methane from shallow seep areas of the NW Svalbard Arctic margin does not reach the sea surface, 17(223259), 223259.

Simstich, J., Sarnthein, M., & Erlenkeuser, H. (2003). Paired δ18O signals of Neogloboquadrina pachyderma (s) and Turborotalita quinqueloba show thermal stratification structure in Nordic Seas. *Marine Micropaleontology*, *48*(1–2), 107–125. https://doi.org/10.1016/S0377-8398(02)00165-2

Spero, H. J., & Lea, D. W. (1996). Experimental determination of stable isotope variability in Globigerina bulloides: Implications for paleoceanographic reconstructions. *Marine Micropaleontology*, *28*(3–4), 231–246.

Spindler, M. (1996). On the salinity tolerance of the planktonic foraminifer neogloboquadrina pachyderma from antarctic sea ice. *Proceedings of the NIPR Symposium on Polar Biology*, *9*, 85–91. https://doi.org/10.2113/gsjfr.21.2.182

Steinle, L., Graves, C. A., Treude, T., Ferré, B., Biastoch, A., Bussmann, I., et al. (2015). Water column methanotrophy controlled by a rapid oceanographic switch. *Nature Geoscience*. https://doi.org/10.1038/NGEO2420

Stouffer, R. J., Manabe, S., & Bryan, K. (1989). Interhemispheric asymmetry in climate response to a gradual increase of atmospheric CO2. *Nature*, *342*(6250), 660–662. https://doi.org/10.1038/342660a0

Stroeve, J. C., Serreze, M. C., Holland, M. M., Kay, J. E., Malanik, J., & Barrett, A. P. (2012). The Arctic's rapidly shrinking sea ice cover: A research synthesis. *Climatic Change*, *110*(3–4), 1005–1027. https://doi.org/10.1007/s10584-011-0101-1

Thomsen, E., Rasmussen, T. L., Sztybor, K., Hanken, N., Tendal, O. S., & Uchman, A. (2019). Cold-seep fossil macrofaunal assemblages from Vestnesa Ridge, eastern Fram Strait, during the past 45 000 years. *Polar Research*, *38*(3310), 1–20. https://doi.org/10.33265/polar.v38.3310

Uppström, L. R. (1974). The boron/chlorinity ratio of deep-sea water from the Pacific Ocean. *Deep-Sea Research and Oceanographic Abstracts*, *21*(2), 161–162. https://doi.org/10.1016/0011-7471(74)90074-6

Vielstädte, L., Karstens, J., Haeckel, M., Schmidt, M., Linke, P., Reimann, S., et al. (2015). Quantification of methane emissions at abandoned gas wells in the Central North Sea. *Marine and Petroleum Geology*, *68*, 848–860. https://doi.org/10.1016/j.marpetgeo.2015.07.030

Volkmann, R. (2000). Planktic foraminifers in the outer Laptev Sea and the Fram Strait—Modern distribution and ecology. *Journal of Foraminiferal Research*, *30*(3), 157–176. https://doi.org/10.2113/0300157

Wang, K., Hunt, B. P. V., Liang, C., Pauly, D., & Pakhomov, E. A. (2017). Reassessment of the life cycle of the pteropod Limacina helicina from a high resolution interannual time series in the temperate North Pacific. *ICES Journal of Marine Science*, *74*(7), 1906–1920. https://doi.org/10.1093/icesjms/fsx014

Wassmann, P., & Slagstad, D. (1993). Seasonal and annual dynamics of particulate carbon flux in the Barents Sea—A model approach. *Polar Biology*, *13*(6), 363–372. https://doi.org/10.1007/BF01681977

Westbrook, G. K., Thatcher, K. E., Rohling, E. J., Piotrowski, A. M., Osborne, A. H., Nisbet, E. G., et al. (2009). Escape of methane gas from the seabed along the West Spitsbergen continental margin. *Geophysical Research Letters*, *36*, L15608. https://doi.org/10.1029/2009GL039191

Wiesenburg, D. A., & Guinasso, N. L. (1979). Equilibrium solubilities of methane, carbon monoxide, and hydrogen in water and sea water. *Journal of Chemical & Engineering Data*, *24*(4), 356–360.